Supporting Information

Self-Limiting Surface Leaching Stabilizes Ru-Based Catalysts for Acidic Water Oxidation

Yang Liu,‡[ab] Xiyu Li,‡[cd] Haeseong Jang,‡[ef] Jianghua Wu,‡[gh] Min Gyu Kim,[f] Xiaoke Xi,[a] Zhanwu Lei,*[a] Yuchen Zhang,[a] Yu Deng,[i] Wensheng Yan,[j] Jun Jiang,[k] Shuhong Jiao,*[k] Jing-Li Luo*[b] and Ruiguo Cao*[a]

[a.] Hefei National Laboratory for Physical Science at the Microscale, Department of Materials Science and Engineering, University of Science and Technology of China, Hefei, 230026, China.

[b.] Shenzhen Key Laboratory of Energy Electrocatalytic Materials, Guangdong Provincial Key Laboratory of New Energy Materials Service Safety, College of Materials Science and Engineering, Shenzhen University, Shenzhen 518055, Guangdong, China.

[c.] School of Physical Sciences, Great Bay University, Dongguan 523000, China.

[d.] Songshan Lake Materials Laboratory, Dongguan, Guangdong, 523808, China.

[e.] Department of Advanced Materials Engineering, Chung-Ang University, Gyeonggi-do, 17546, Republic of Korea.

[f.] Department of Intelligent Energy and Industry, Chung-Ang University, 84 Heukseok-ro, Dongjak-gu, Seoul 06974, Republic of Korea.

[g.] Department of Chemistry, Guangdong Provincial Key Laboratory of Catalysis, Southern University of Science and Technology, Shenzhen 518055, China.

[h.] Suzhou Institute of Nano-Tech and Nano-Bionics (SINANO), Chinese Academy of Sciences, Suzhou 215123, China.

[i.] National Laboratory of Solid-State Microstructures, Jiangsu Key Laboratory of Artificial Functional Materials, College of Engineering and Applied Sciences and Collaborative Innovation Center of Advanced Microstructures, Nanjing University, Nanjing 210093, China.

[j.] National Synchrotron Radiation Laboratory, University of Science and Technology of China, Hefei, 230029, China.

[k.] Key Laboratory of Precision and Intelligent Chemistry, University of Science and Technology of China, Hefei, 230026, China

‡ These authors contributed equally to this work.

E-mail: zwlei@mail.ustc.edu.cn, jiaosh@ustc.edu.cn, jingli.luo@ualberta.ca, rgcao@ustc.edu.cn

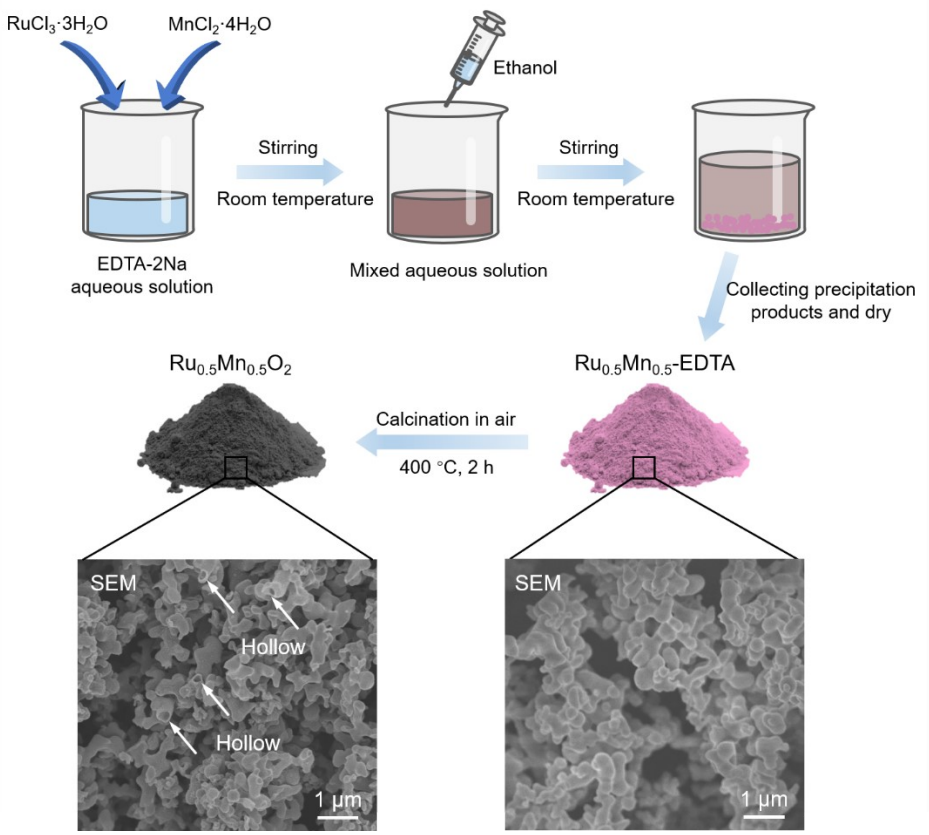

Figure S1. Schematic route for synthesis of $Ru_{0.5}Mn_{0.5}O_2$ solid solution.

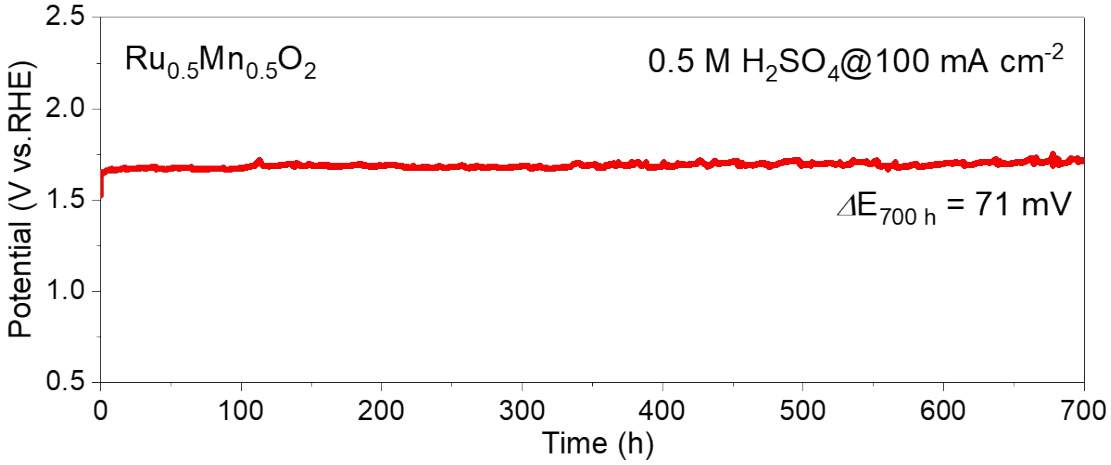

Figure S2. Chronopotentiometry stability test of $Ru_{0.5}Mn_{0.5}O_2$ for OER at 100 mA cm^{-2} in 0.5 M H_2SO_4.

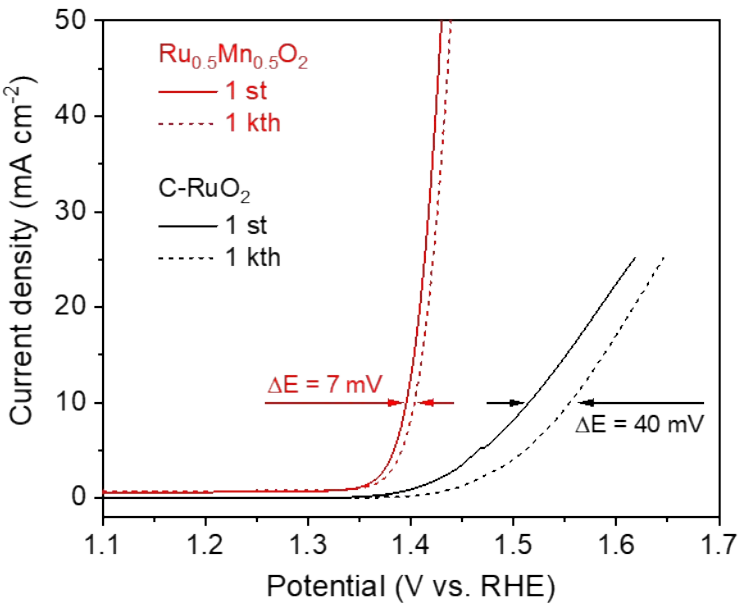

Figure S3. Polarization curves of $Ru_{0.5}Mn_{0.5}O_2$ and C-RuO_2 for the 1st and 1 kth CV scans.

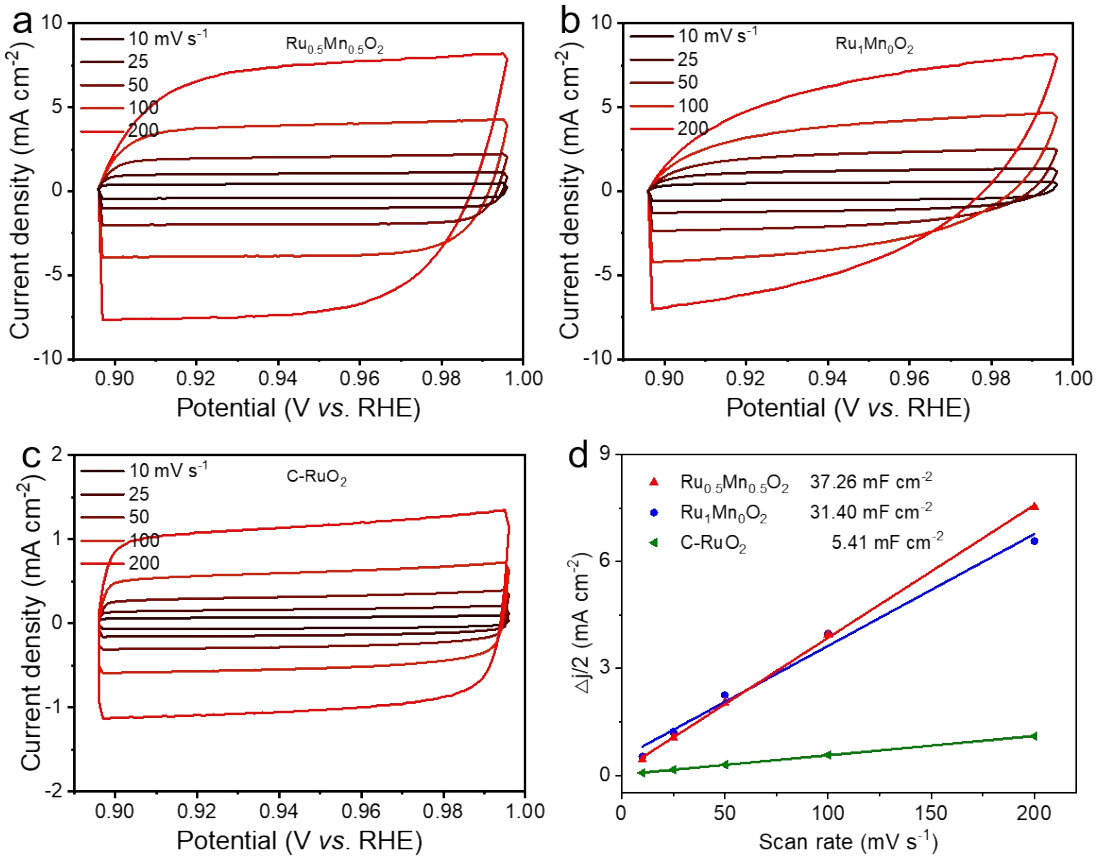

Figure S4. CV curves of $Ru_{0.5}Mn_{0.5}O_2$ (**a**), $Ru_1Mn_0O_2$ (**b**), and C-RuO_2 (**c**). The CV measurements were conducted in a non-Faradaic region of the voltammogram at various scan rates: 10, 25, 50, 100, and 200 mV s^{-1}. **(d)** C_{dl} values were estimated through linear fitting of the scan rate for $Ru_{0.5}Mn_{0.5}O_2$, $Ru_1Mn_0O_2$, and C-RuO_2.

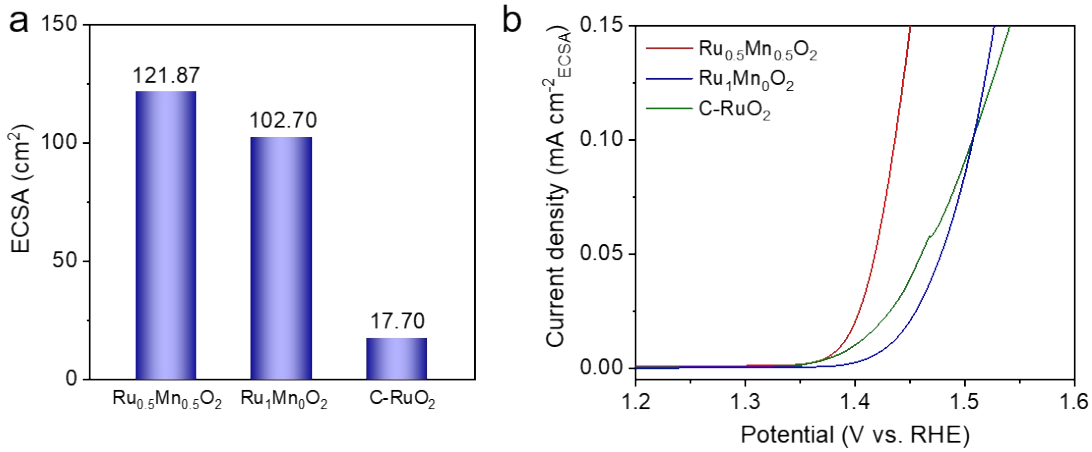

Figure S5. (a) ECSA of $Ru_{0.5}Mn_{0.5}O_2$, $Ru_1Mn_0O_2$, and C-RuO_2. (b) Normalized LSV curves for intrinsic activity assessment.

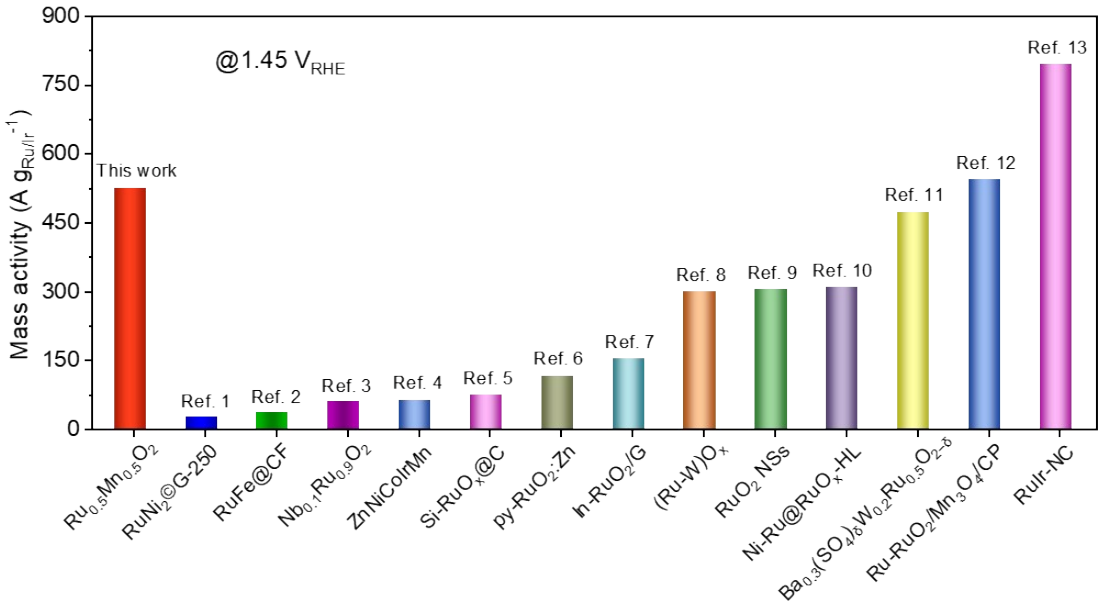

Figure S6. Comparison of the normalized mass activities of $Ru_{0.5}Mn_{0.5}O_2$ and recently reported Ru- or Ir-based acidic OER catalysts at 1.45 V vs. RHE.

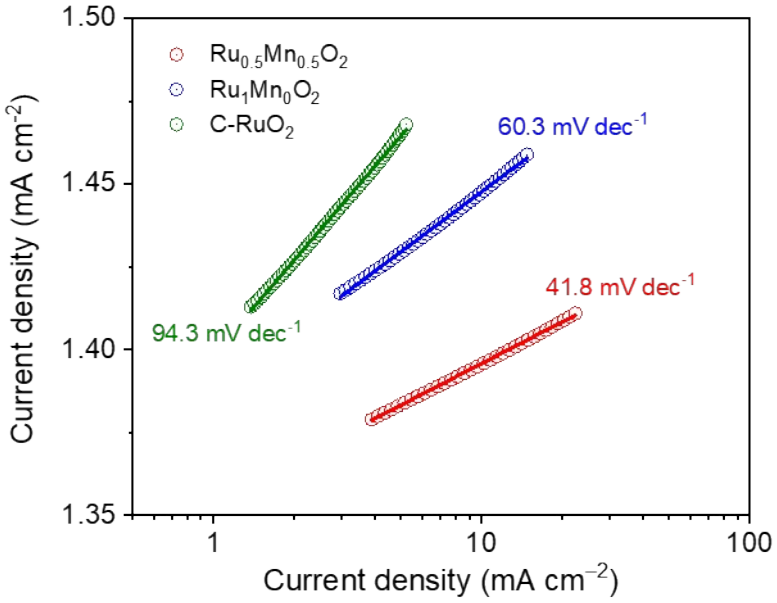

Figure S7. Tafel slopes for $Ru_{0.5}Mn_{0.5}O_2$, $Ru_1Mn_0O_2$, and C-RuO_2.

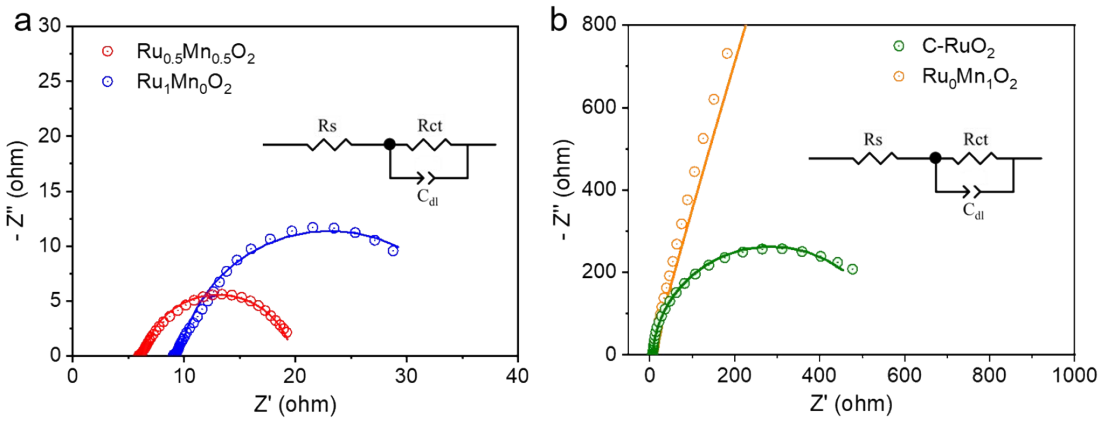

Figure S8. Nyquist plots of (**a**) $Ru_{0.5}Mn_{0.5}O_2$, $Ru_1Mn_0O_2$, and (**b**) $Ru_0Mn_1O_2$, C-RuO_2 at 1.42 V vs. RHE. Solid curves are the fitting results by using the equivalent circuit shown in the inset, where the charge transfer resistance and the intrinsic electrode and electrolyte resistances are denoted as R_{ct} and R_s, respectively.

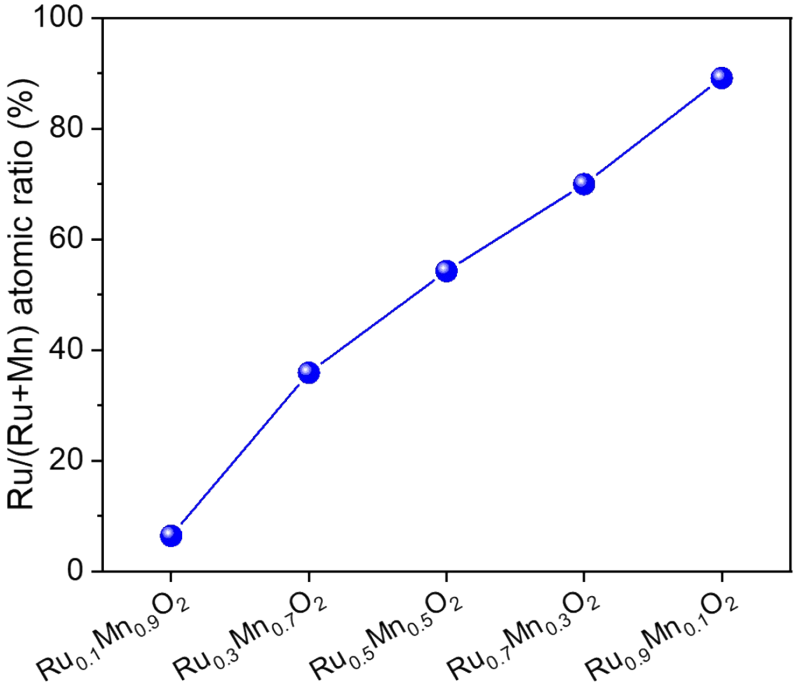

Figure S9. The Ru/(Ru+Mn) atomic ratios in $Ru_yMn_{1-y}O_2$ (y=0.1, 0.3, 0.5, 0.7, and 0.9) according to ICP-AES analysis.

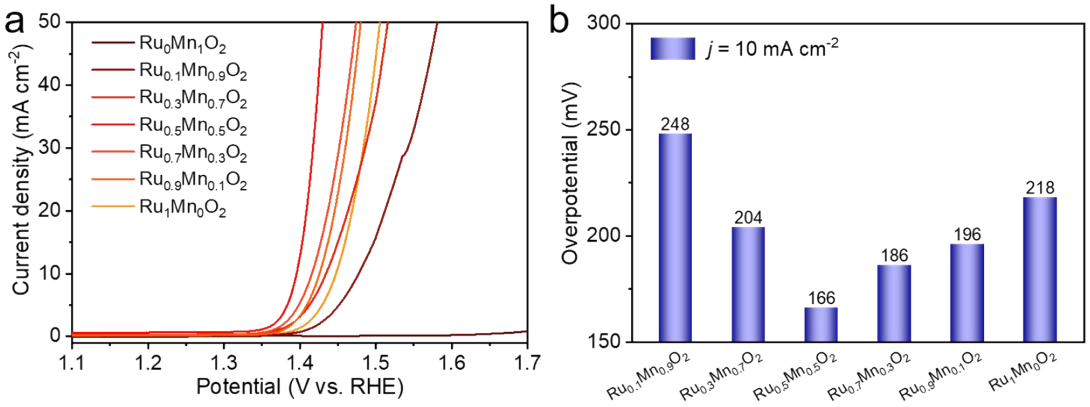

Figure S10. (a) LSV curves of $Ru_yMn_{1-y}O_2$ (y = 0, 0.1, 0.3, 0.5, 0.7, 0.9, and 1). (b) Overpotential to reach 10 mA cm $^{-2}$ for these catalysts.

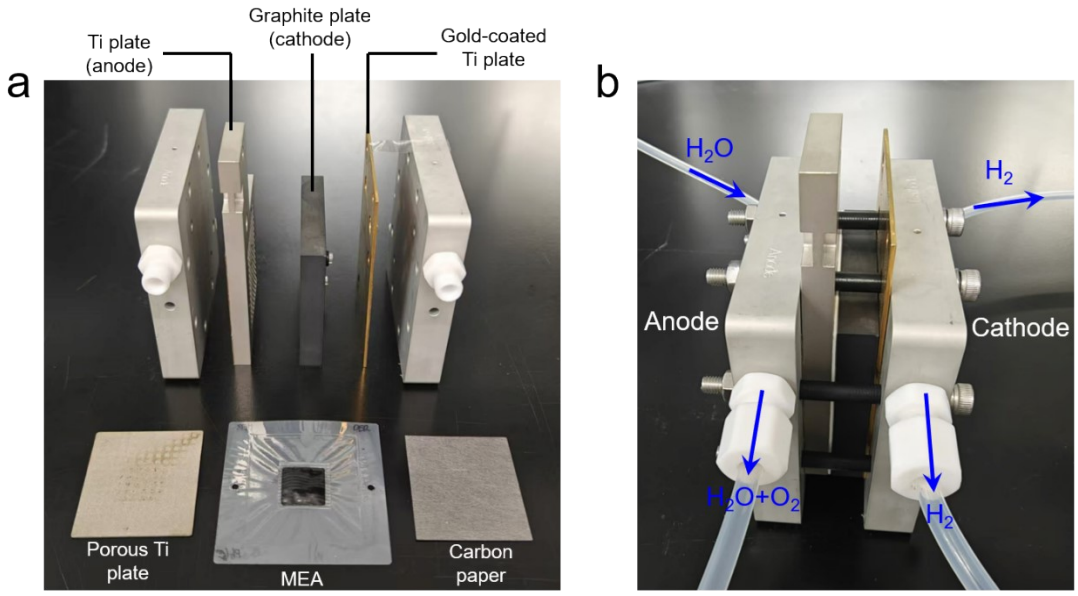

Figure S11. (a) Optical photo of the component of a PEM electrolyzer. (b) Optical photo of the assembled PEM electrolyzer.

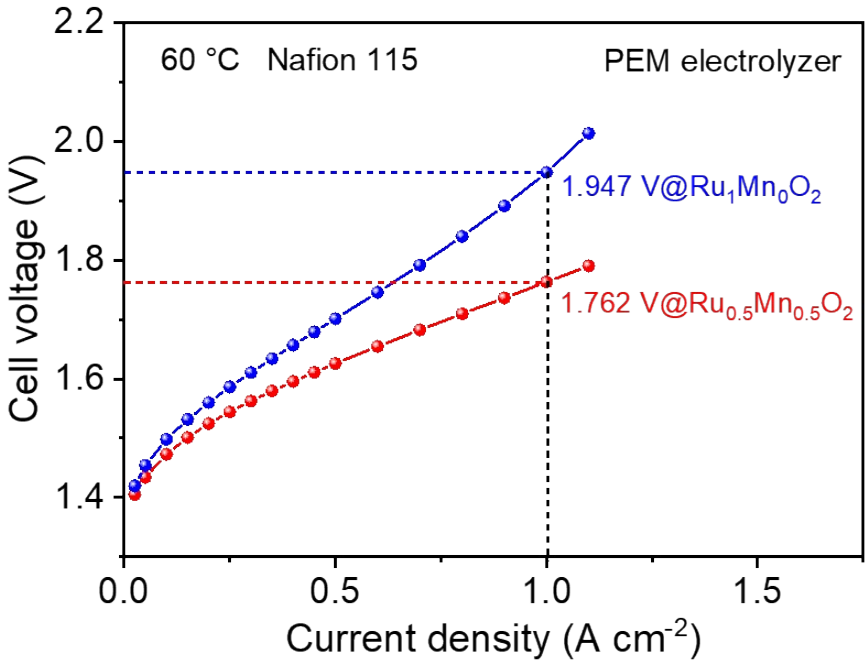

Figure S12. Polarization curves of PEM electrolyzers using $Ru_{0.5}Mn_{0.5}O_2$ or $Ru_1Mn_0O_2$ as anodic catalyst and commercial Pt/C as cathodic catalyst at 60 °C. No cell voltages were iR compensated.

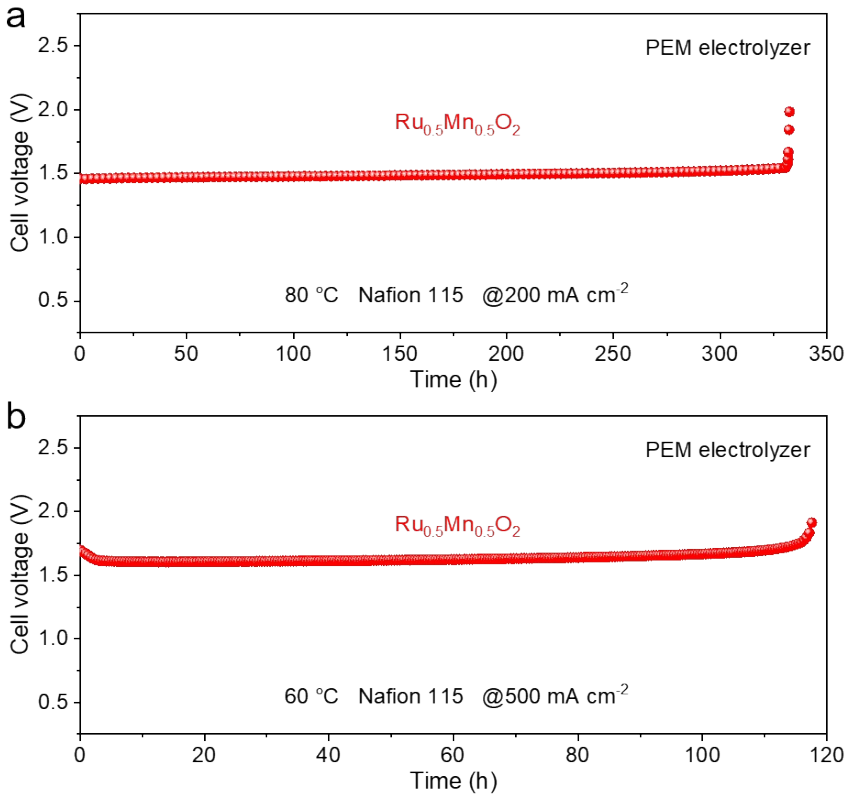

Figure S13. Chronopotentiometry testing of PEM electrolyzers using $Ru_{0.5}Mn_{0.5}O_2$ as anodic catalyst and commercial Pt/C as cathodic catalyst operated at 200 mA cm^{-2} at 80 °C (a) and 500 mA cm^{-2} at 60 °C (b).

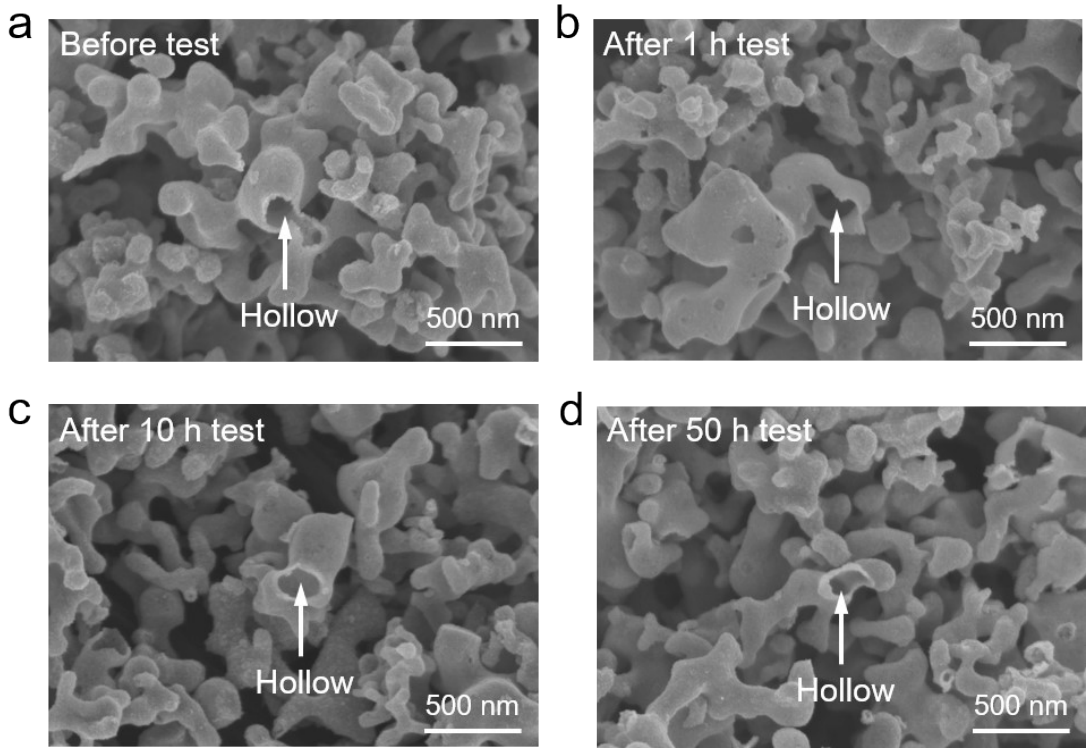

Figure S14. SEM images of $Ru_{0.5}Mn_{0.5}O_2$ catalysts before test (a) and after 1 h test (b), after 10 h test (c), after 50 h test (d).

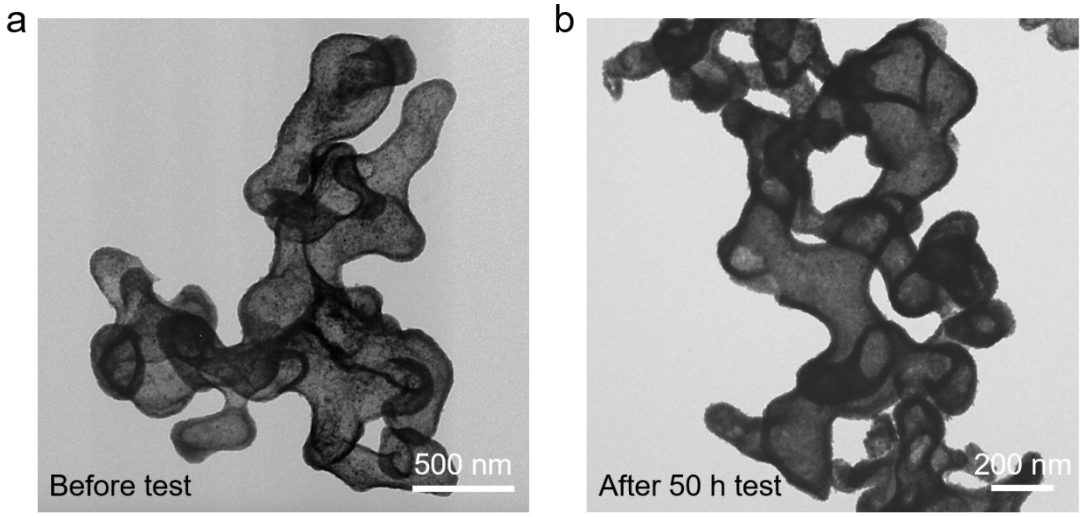

Figure S15. Low-magnification TEM image of $Ru_{0.5}Mn_{0.5}O_2$ catalysts before test (a) and after 50 h test (b).

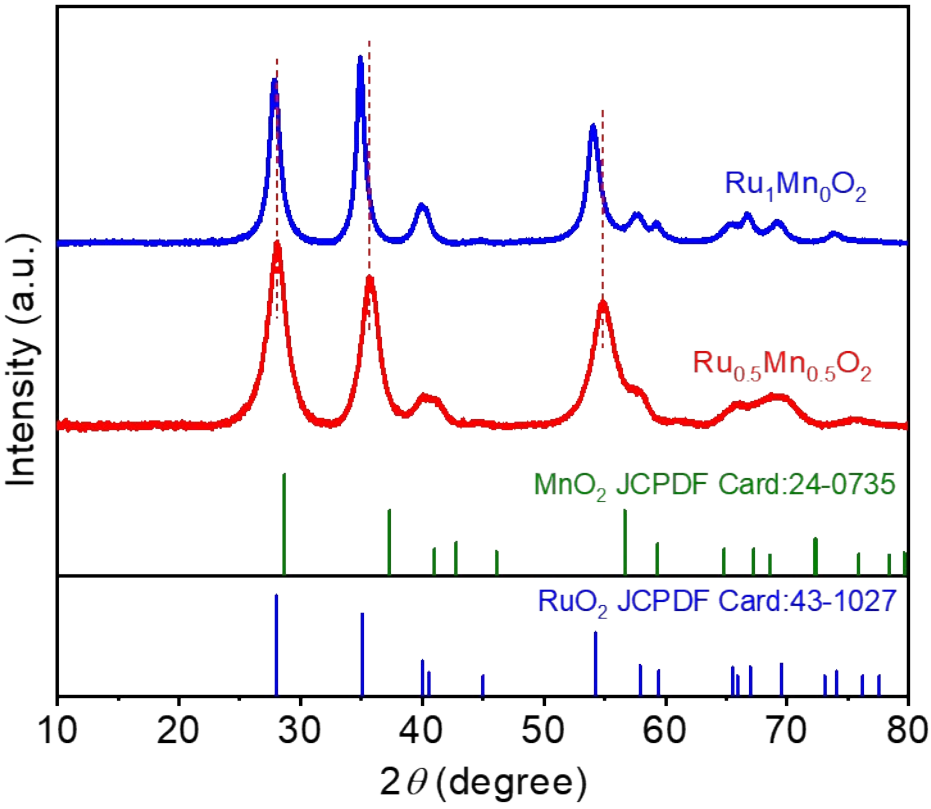

Figure S16. XRD patterns of $Ru_{0.5}Mn_{0.5}O_2$ and $Ru_1Mn_0O_2$.

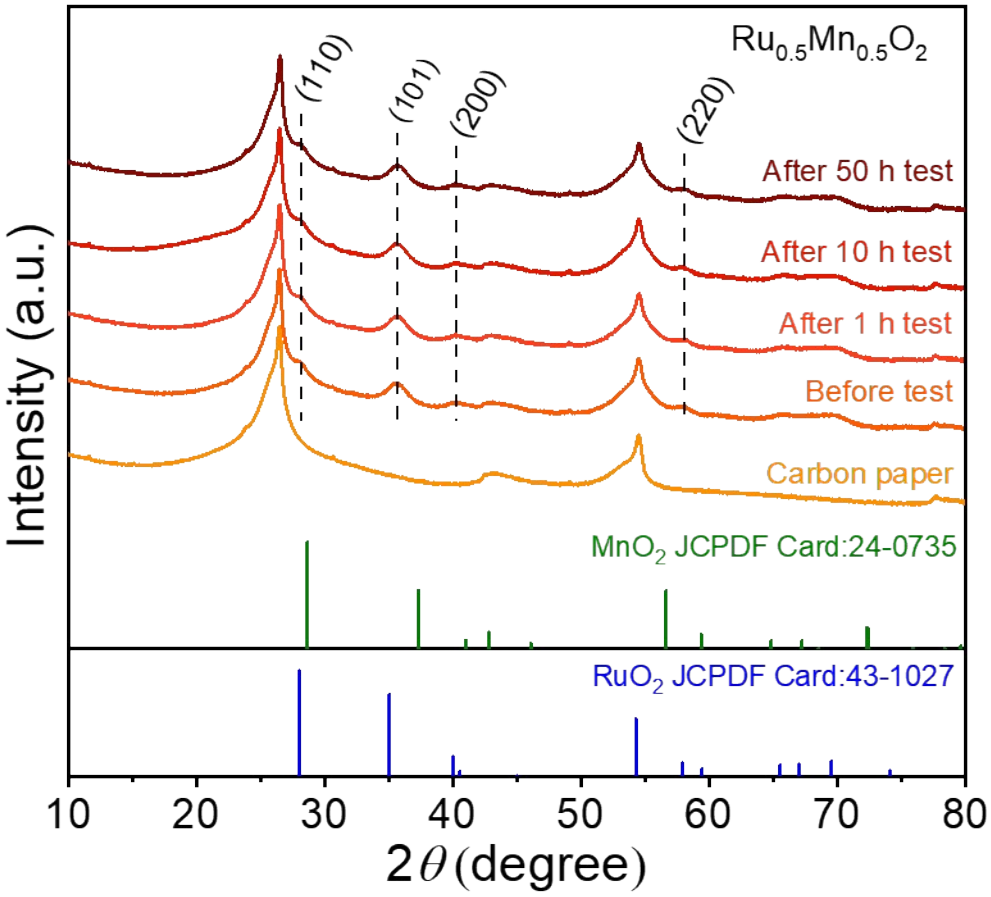

Figure S17. XRD patterns of $Ru_{0.5}Mn_{0.5}O_2$ loaded on carbon paper before and after 1 h, 10 h, 50 h OER test.

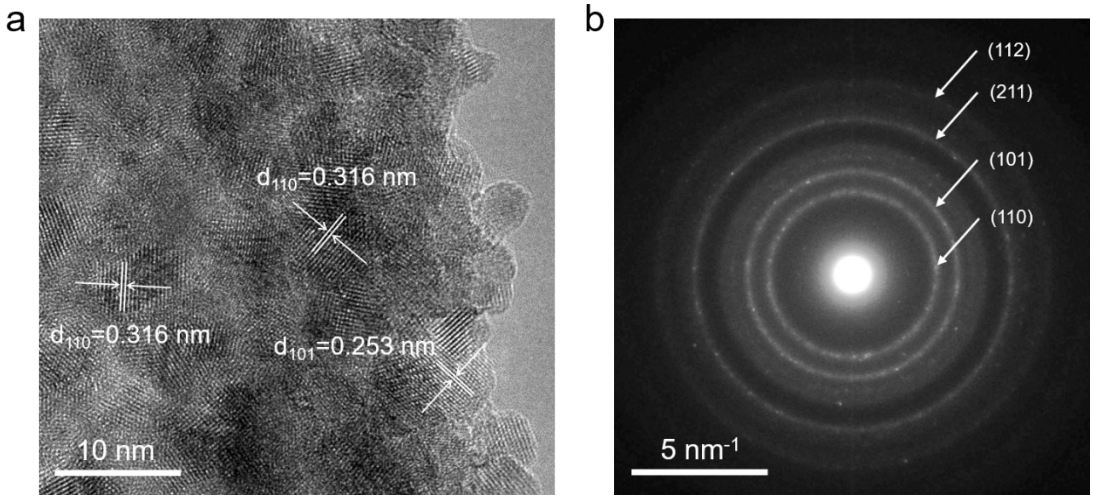

Figure S18. (a) HRTEM image of $Ru_{0.5}Mn_{0.5}O_2$. (b) SAED pattern of $Ru_{0.5}Mn_{0.5}O_2$.

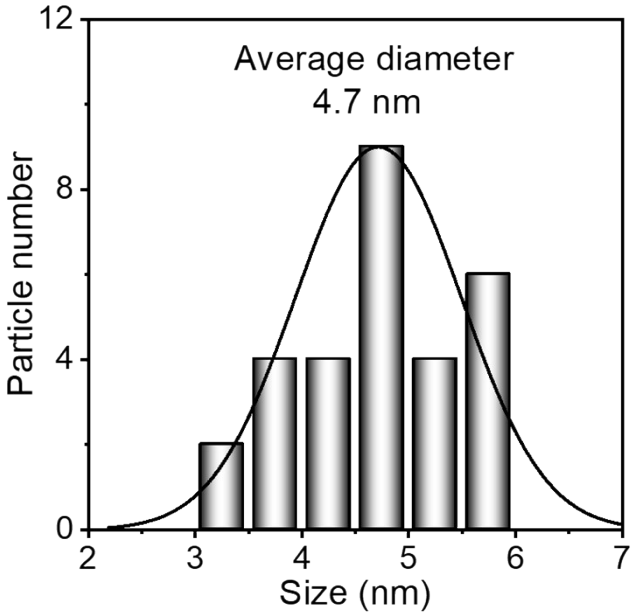

Figure S19. Particle size distribution of $Ru_{0.5}Mn_{0.5}O_2$.

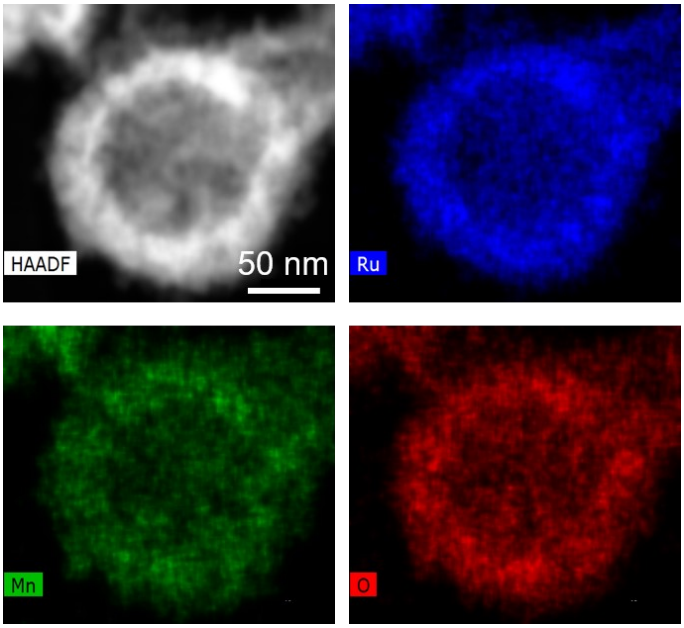

Figure S20. HAADF image of $Ru_{0.5}Mn_{0.5}O_2$ and the corresponding EDS elemental mappings of Ru, Mn, and O.

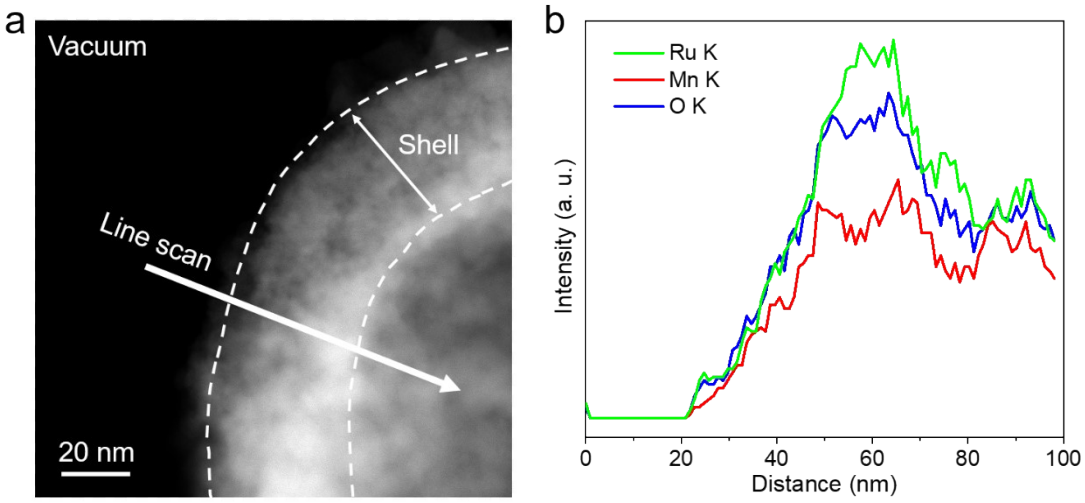

Figure S21. (a) HAADF image of $Ru_{0.5}Mn_{0.5}O_2$ after 50 h test with an arrow indicating the EDX line scan position. (b) EDX line scan with Ru K_α signal, Mn K_α signal, and O K_α signal of the hollow shell structure shown in (a).

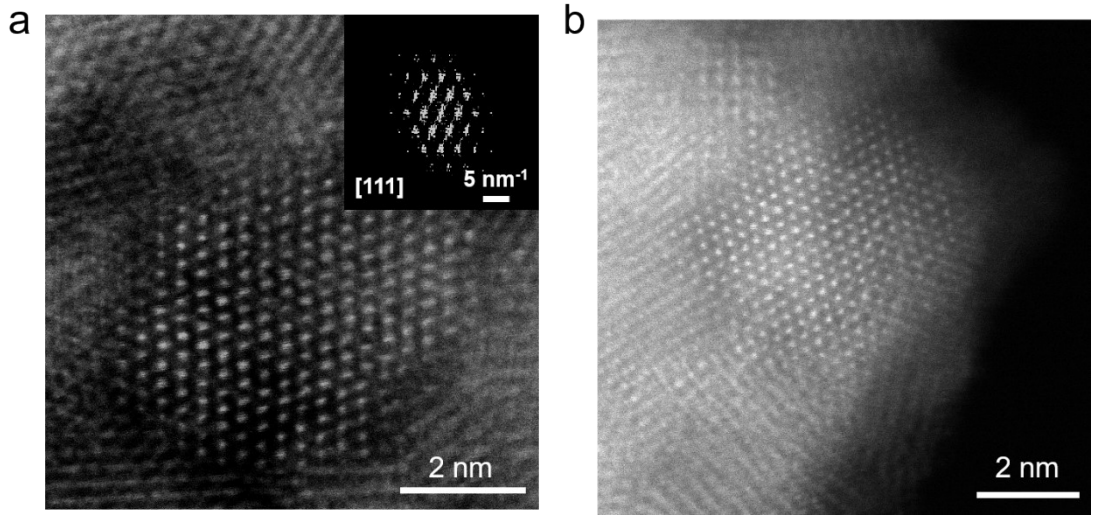

Figure S22. (a) Atomic-resolution HAADF-STEM image of $Ru_{0.5}Mn_{0.5}O_2$ and corresponding FFT pattern. (b) Atomic-resolution HAADF-STEM image of particles located in the surface area.

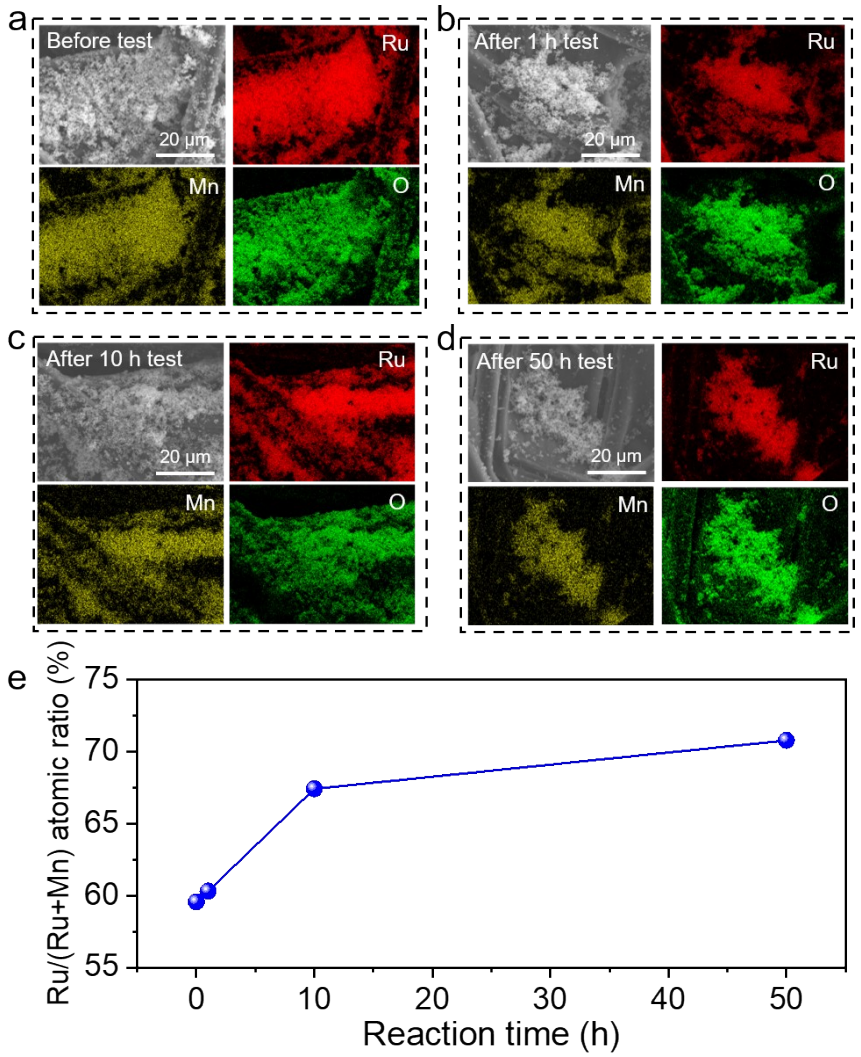

Figure S23. (a) SEM image of $Ru_{0.5}Mn_{0.5}O_2$ loaded on carbon paper and the corresponding EDS elemental mappings. (b) SEM image of $Ru_{0.5}Mn_{0.5}O_2$ after 1 h test and the corresponding EDS elemental mappings. (c) SEM image of $Ru_{0.5}Mn_{0.5}O_2$ after 10 h test and the corresponding EDS elemental mappings. (d) SEM image of $Ru_{0.5}Mn_{0.5}O_2$ after 50 h test and the corresponding EDS elemental mappings. (e) The atomic ratio of Ru/(Ru+Mn) in $Ru_{0.5}Mn_{0.5}O_2$ before test, after 1 h test, after 10 h test, and after 50 h test according to EDS analysis.

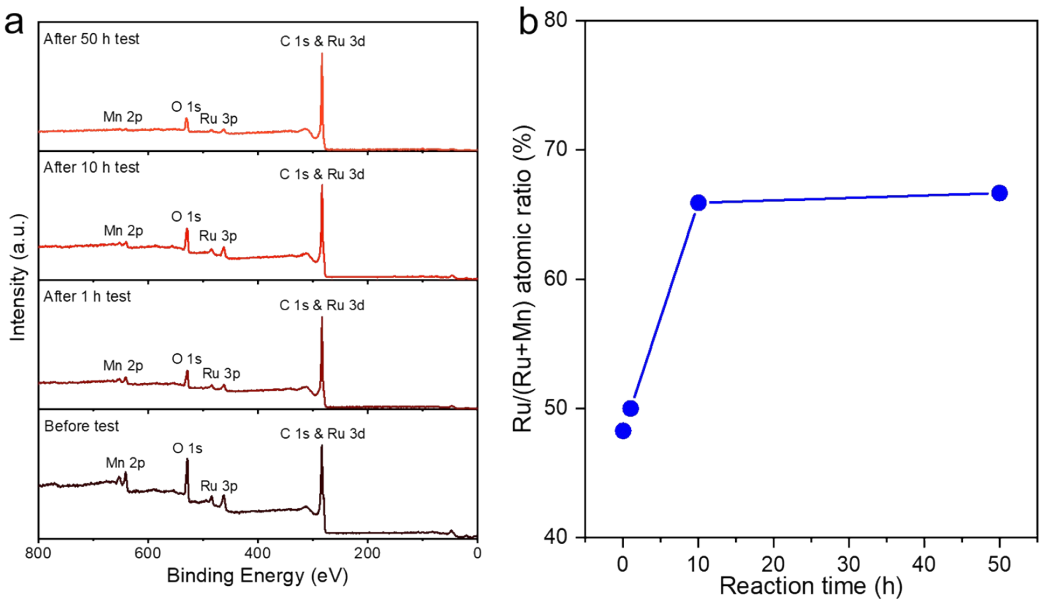

Figure S24. (a) XPS full scan spectrum of $Ru_{0.5}Mn_{0.5}O_2$ loaded on carbon paper before and after 1 h, 10 h, 50 h OER test. (b) The atomic ratio of Ru/(Ru+Mn) in $Ru_{0.5}Mn_{0.5}O_2$ before test, after 1 h test, after 10 h test, and after 50 h test according to XPS analysis.

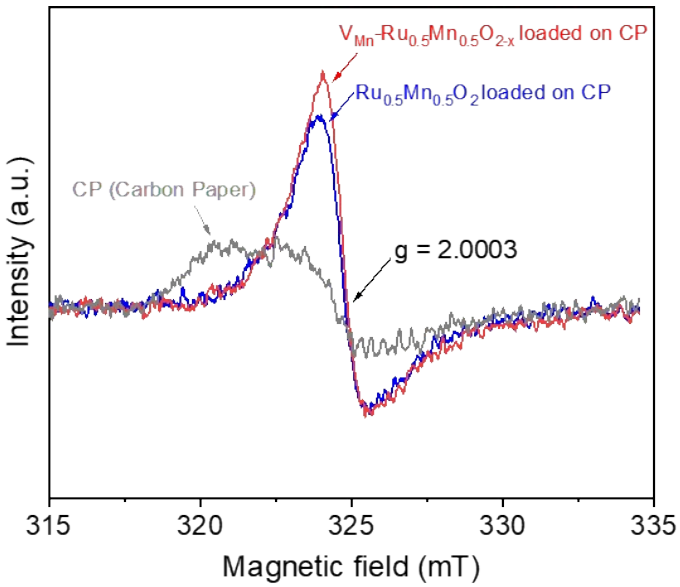

Figure S25. EPR spectra of $Ru_{0.5}Mn_{0.5}O_2$ loaded on CP, V_{Mn}-$Ru_{0.5}Mn_{0.5}O_{2-x}$ loaded on CP, and CP (carbon paper).

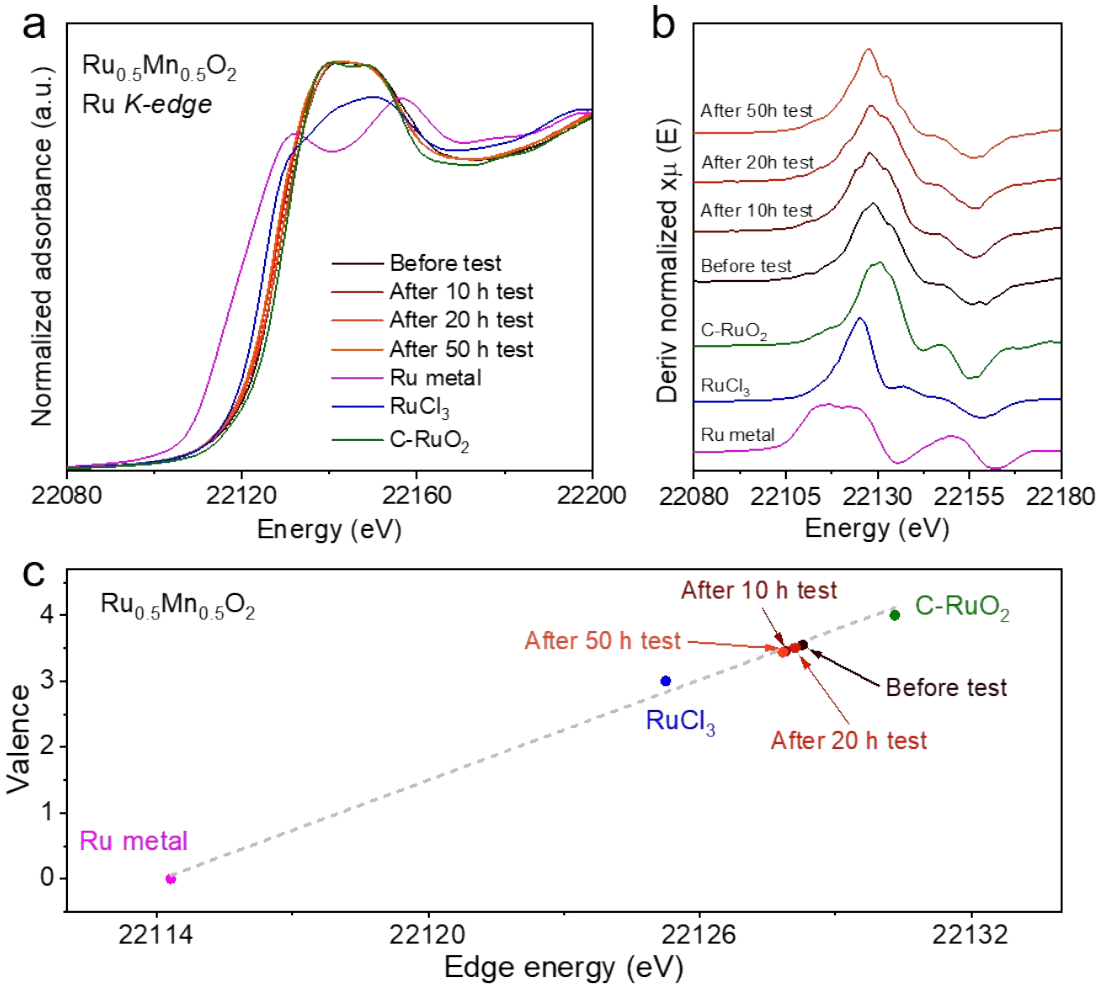

Figure S26. (a) Ru K-edge XANES spectra of reference samples and $Ru_{0.5}Mn_{0.5}O_2$ before test, after 10 h test, after 20 h test, after 50 h test. (b) The corresponding derivative of XANES spectra. (c) The relationship between Ru K-edge energy and oxidation state for these catalysts.

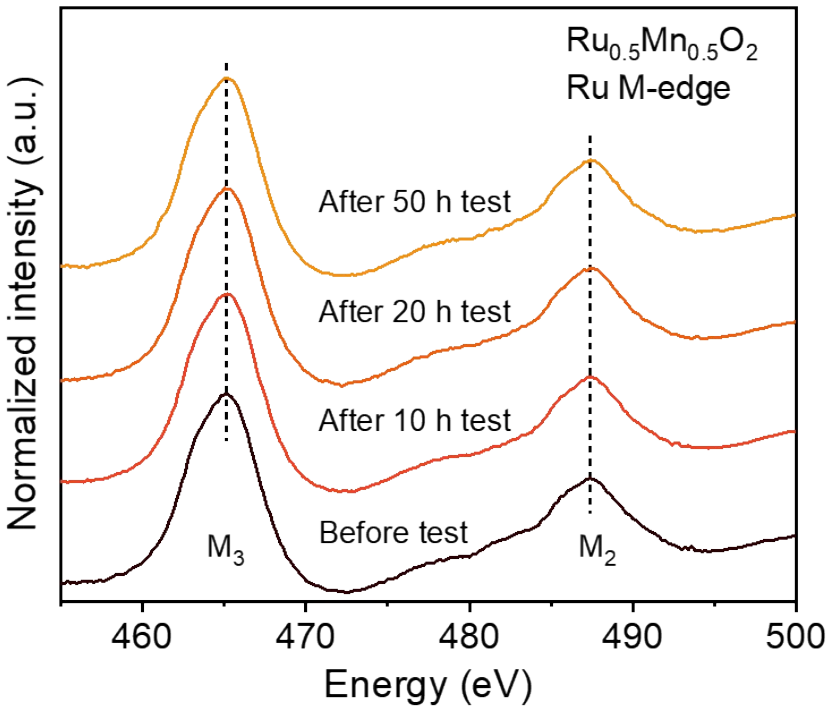

Figure S27. Ru M-edge soft XAS spectra for $Ru_{0.5}Mn_{0.5}O_2$ catalyst before test, after 10 h test, after 20 h test, and after 50 h test.

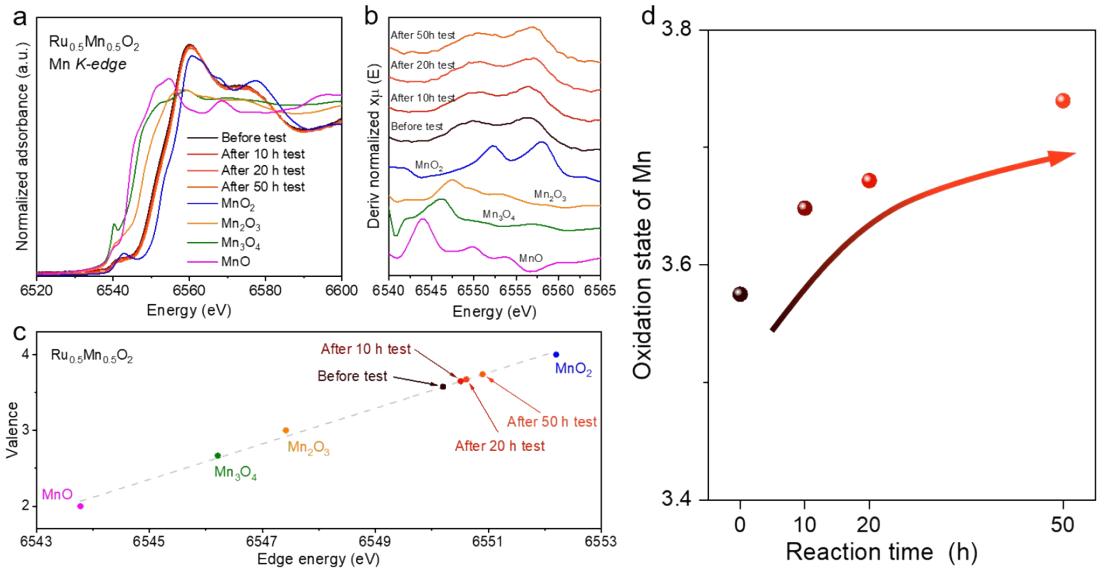

Figure S28. (a) Mn K-edge XANES spectra of reference samples and $Ru_{0.5}Mn_{0.5}O_2$ before test, after 10 h test, after 20 h test, after 50 h test. (b) The corresponding derivative of XANES spectra. (c) The relationship between Mn K-edge energy and oxidation state for these catalysts. (d) The valence state of Mn under different reaction time.

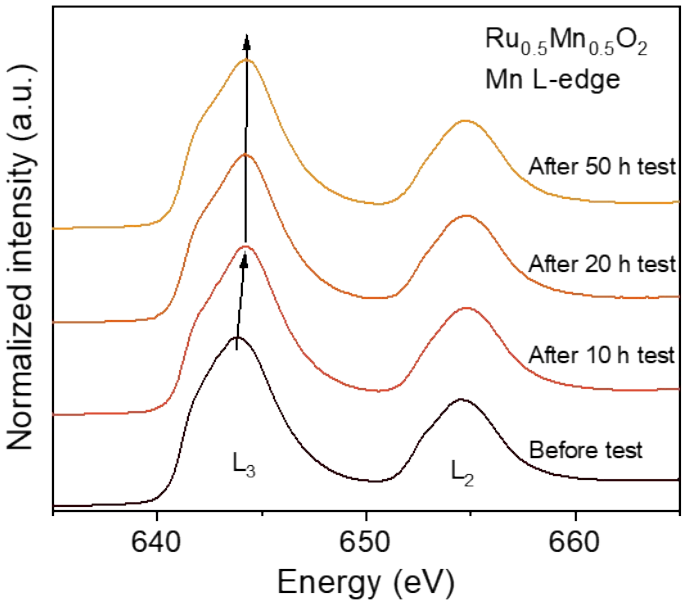

Figure S29. Mn L-edge soft XAS spectra for $Ru_{0.5}Mn_{0.5}O_2$ catalyst before test, after 10 h test, after 20 h test, and after 50 h test.

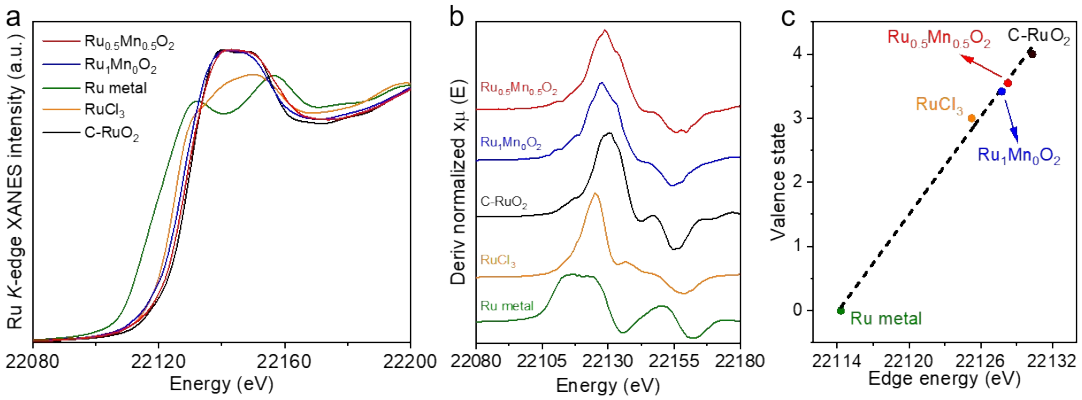

Figure S30. (a) Ru K-edge XANES spectra of $Ru_{0.5}Mn_{0.5}O_2$, $Ru_1Mn_0O_2$, and reference samples. (b) The corresponding derivative of XANES spectra. (c) The relationship between Ru K-edge energy and valence state for $Ru_{0.5}Mn_{0.5}O_2$, $Ru_1Mn_0O_2$, and reference samples.

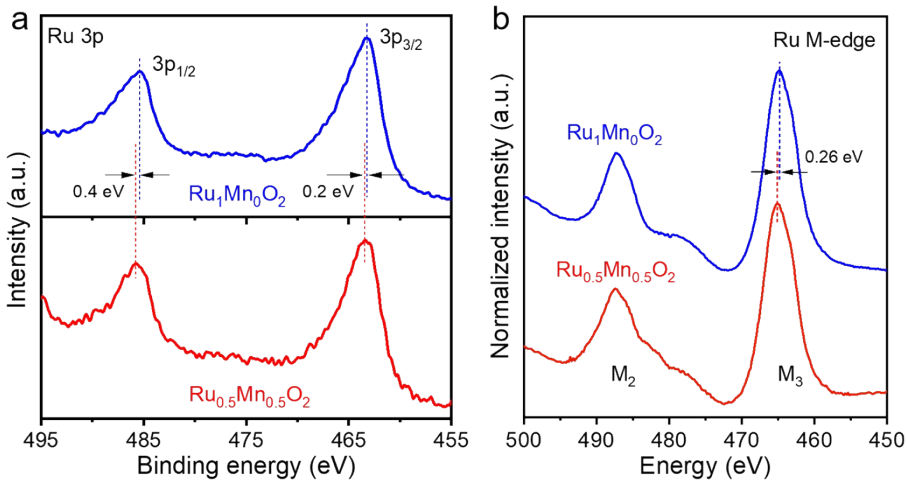

Figure S31. (a) Ru 3p XPS spectra of $Ru_{0.5}Mn_{0.5}O_2$ and $Ru_1Mn_0O_2$. (b) Ru M-edge soft XAS spectra of $Ru_{0.5}Mn_{0.5}O_2$ and $Ru_1Mn_0O_2$.

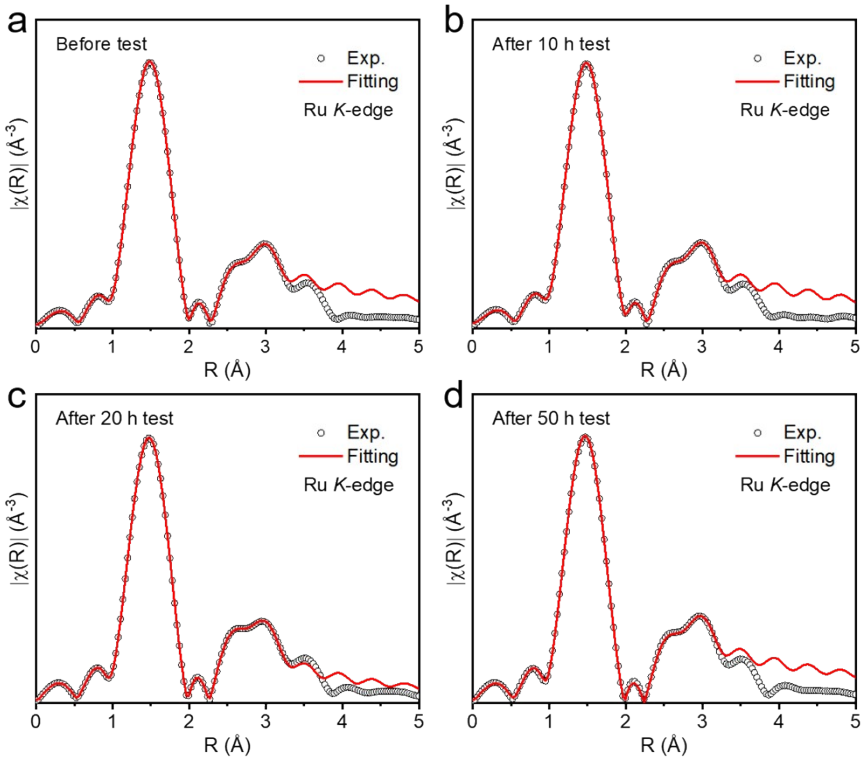

Figure S32. The experimental and fitting curves of FT-EXAFS for $Ru_{0.5}Mn_{0.5}O_2$ catalyst before test (a), after 10 h test (b), after 20 h test (c), and after 50 h test (d) using Ru-O and Ru-M (M=Ru or Co) path.

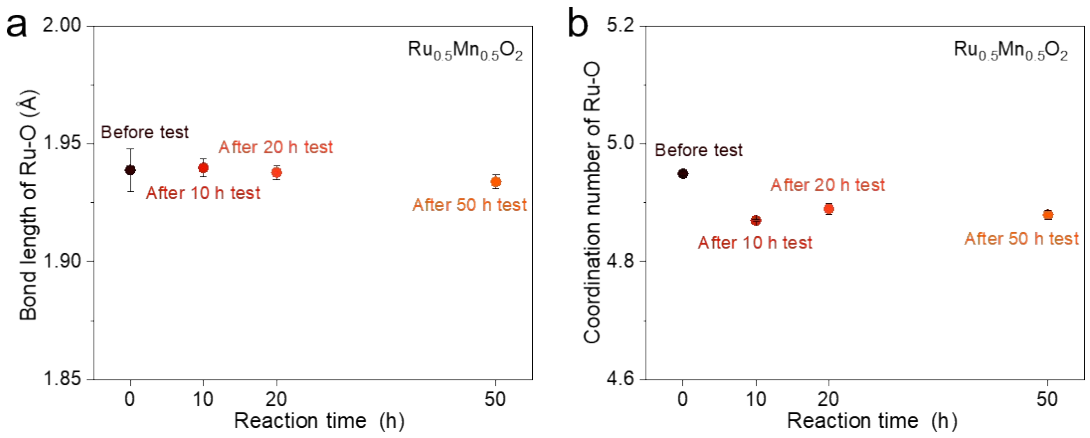

Figure S33. The bond length (**a**) and CN (**b**) of Ru-O for $Ru_{0.5}Mn_{0.5}O_2$ catalyst before and after 10 h, 20 h, 50 h test.

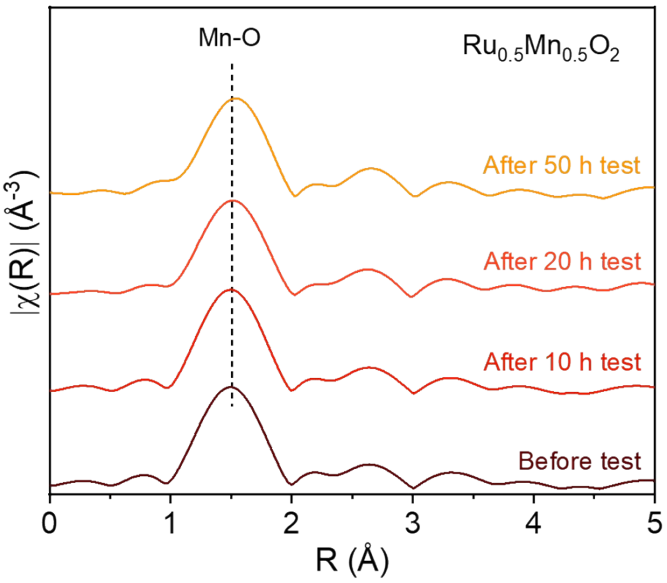

Figure S34. FT-EXAFS spectra at Mn K-edge of $Ru_{0.5}Mn_{0.5}O_2$ before test, after 10 h test, after 20 h test, and after 50 h test.

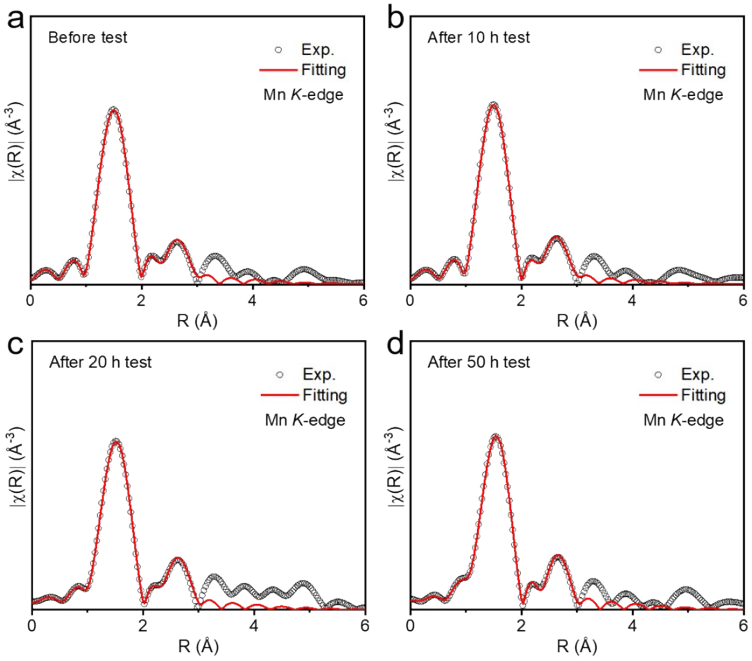

Figure S35. The experimental and fitting curves of FT-EXAFS for $Ru_{0.5}Mn_{0.5}O_2$ catalyst before test (a), after 10 h test (b), after 20 h test (c), and after 50 h test (d) using Mn-O and Mn-M (M=Ru or Mn) path.

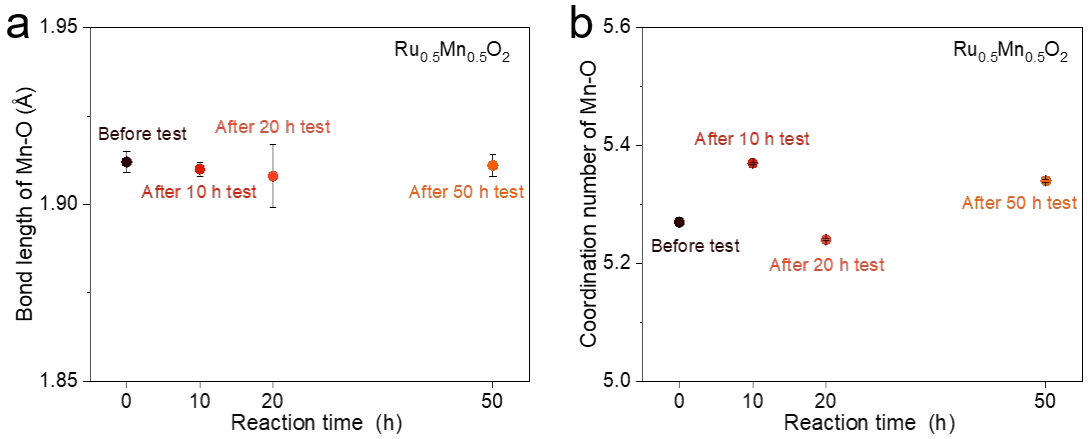

Figure S36. The bond length (**a**) and CN (**b**) of Mn-O for $Ru_{0.5}Mn_{0.5}O_2$ catalyst before and after 10 h, 20 h, 50 h test.

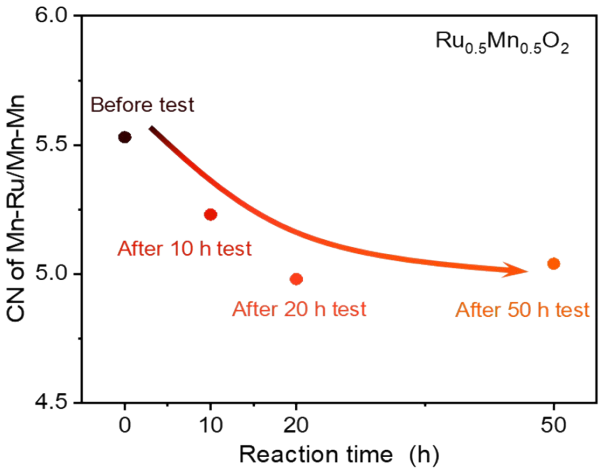

Figure S37. The coordination number of Mn-Ru/Mn-Mn for $Ru_{0.5}Mn_{0.5}O_2$ before and after 10 h, 20 h, 50 h OER test according to Mn K-edge EXAFS fitting.

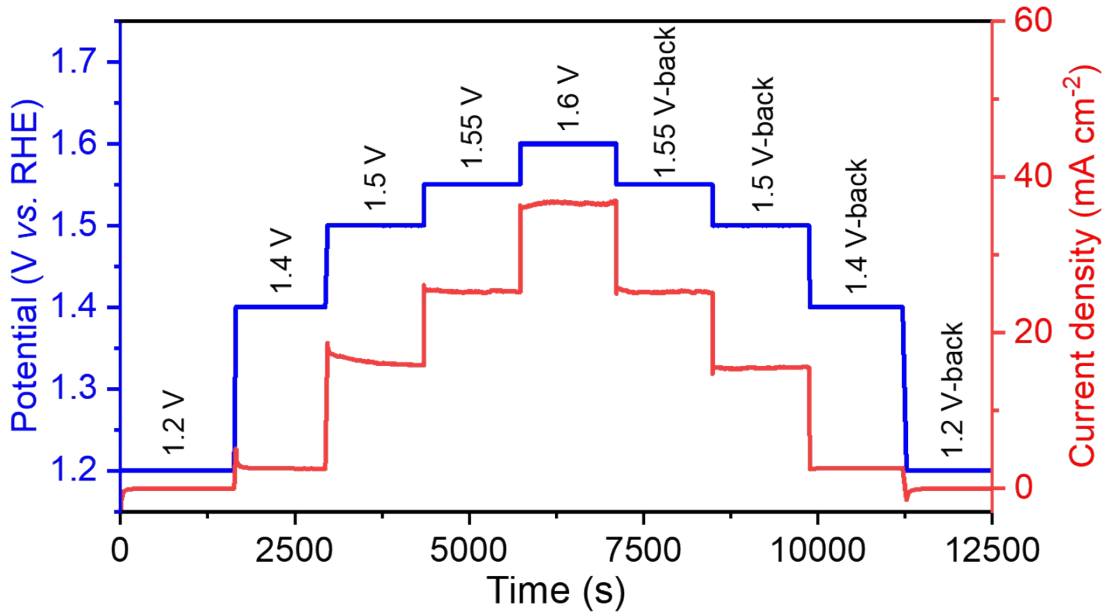

Figure S38. Obtained chronoamperometric profile during operando XAFS measurements. The applied voltage range includes: 1.2 V → 1.4 V → 1.5 V → 1.55 V → 1.6 V → 1.55 V → 1.5 V → 1.4 V → 1.2 V (vs. RHE).

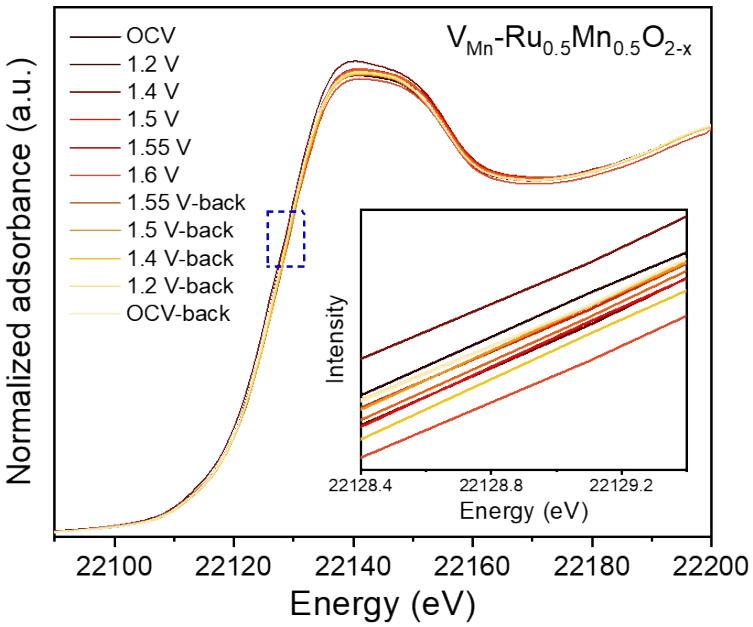

Figure S39. Ru K-edge XANES spectra of V_{Mn}-$Ru_{0.5}Mn_{0.5}O_{2-x}$ under different applied potentials. The insert is an enlarged view of the blue rectangular region.

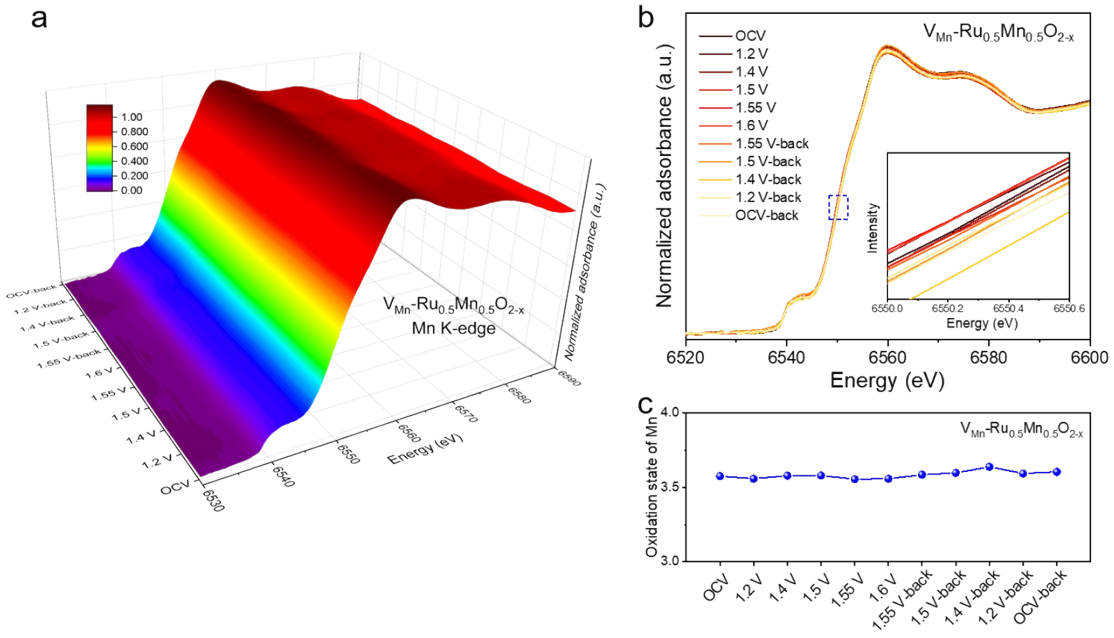

Figure S40. (a) 3D plot of operando Mn K-edge XANES spectra for V_{Mn}-$Ru_{0.5}Mn_{0.5}O_{2-x}$. (b) Mn K-edge XANES spectra under different applied potentials. The insert is an enlarged view of the blue rectangular region. (c) The valence state of Mn under different applied potentials for V_{Mn}-$Ru_{0.5}Mn_{0.5}O_{2-x}$.

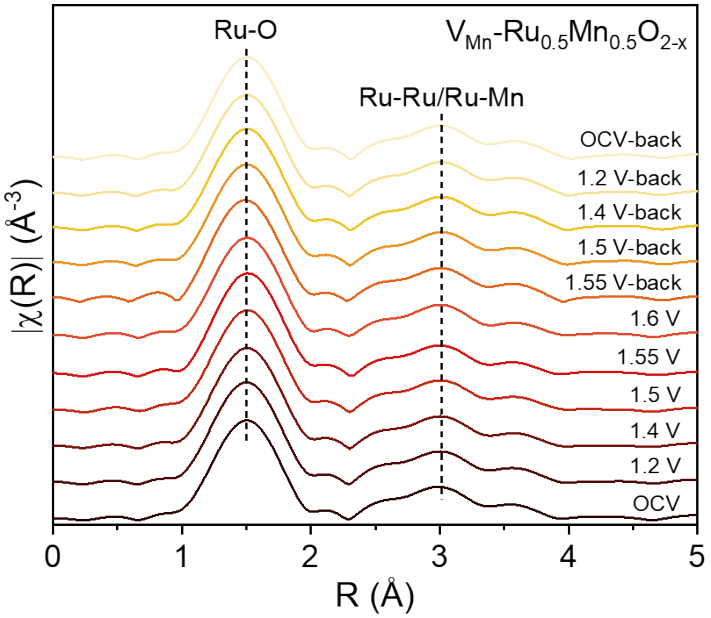

Figure S41. Fourier-transformed Ru K-edge EXAFS spectra of V_{Mn}-$Ru_{0.5}Mn_{0.5}O_{2-x}$ under different applied potentials.

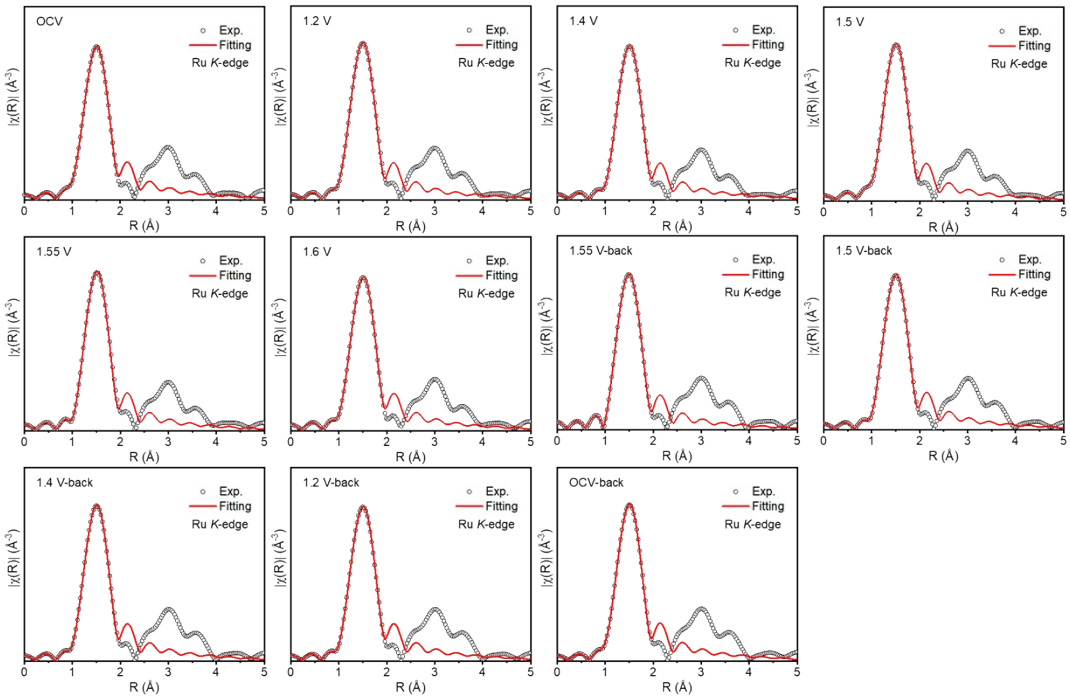

Figure S42. The experimental and fitting curves of FT-EXAFS for V_{Mn}-$Ru_{0.5}Mn_{0.5}O_{2-x}$ under different potentials using Ru-O path.

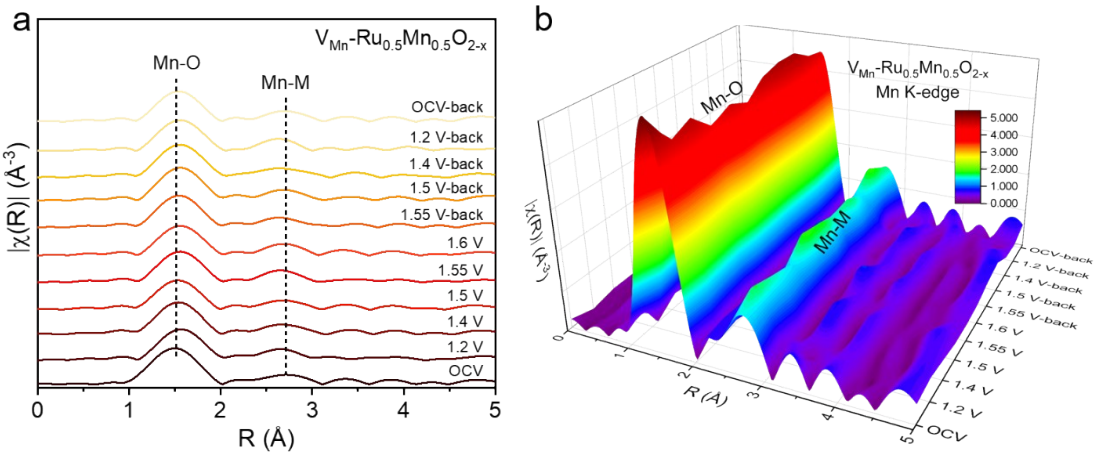

Figure S43. (a) Fourier-transformed Mn K-edge EXAFS spectra of V_{Mn}-$Ru_{0.5}Mn_{0.5}O_{2-x}$ under different applied potentials. (b) The corresponding 3D plot.

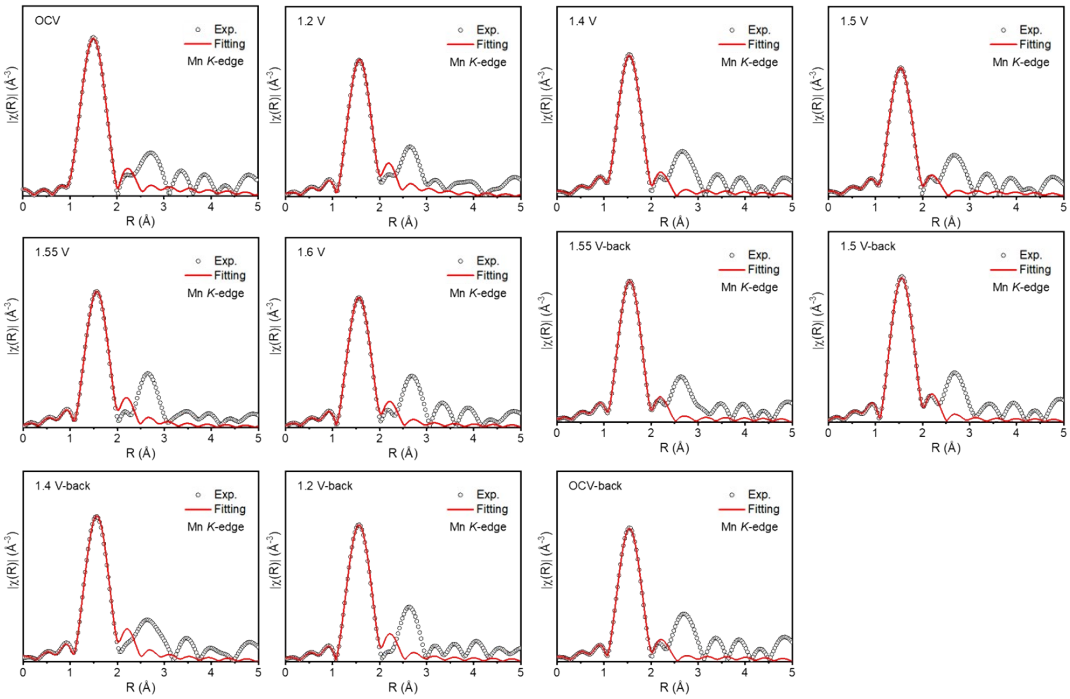

Figure S44. The experimental and fitting curves of FT-EXAFS for V_{Mn}-$Ru_{0.5}Mn_{0.5}O_{2-x}$ under different potentials using Mn-O path.

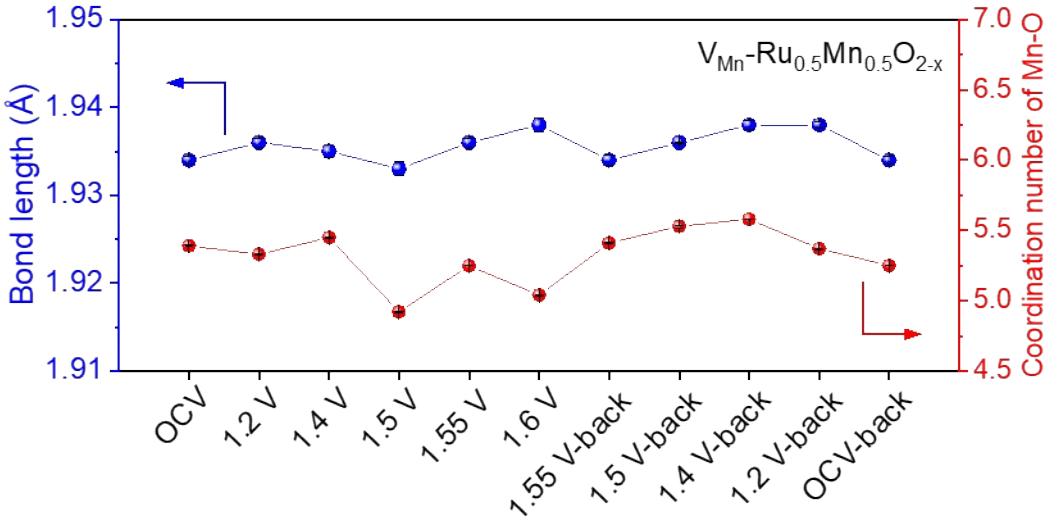

Figure S45. The bond length and CN of Mn-O under different applied potentials according to EXAFS fitting results of V_{Mn}-$Ru_{0.5}Mn_{0.5}O_{2-x}$.

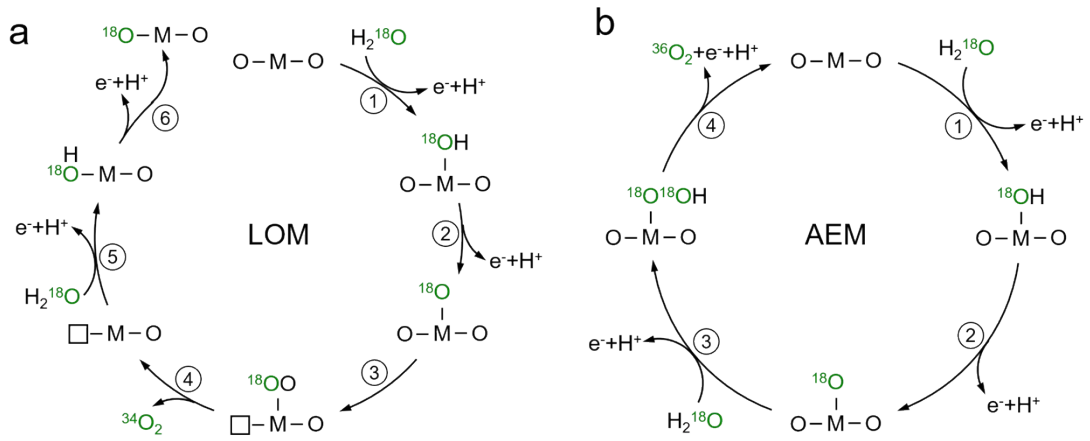

Figure S46. Reaction paths of LOM (a) and AEM (b) in the electrolyte using $H_2{}^{18}O$ as solvent.

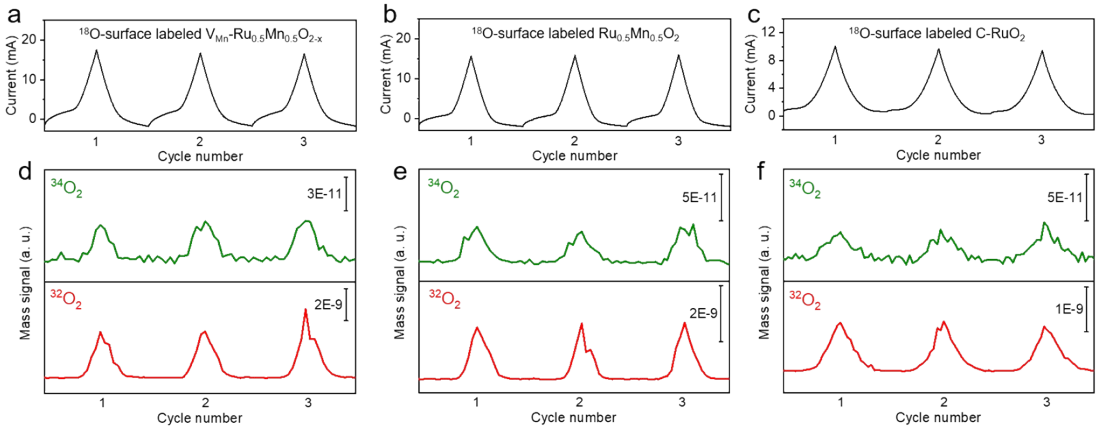

Figure S47. OER reaction current as a function of time during three times of CV in operando DEMS measurement for ^{18}O-surface labeled V_{Mn}-$Ru_{0.5}Mn_{0.5}O_{2-x}$ (a), ^{18}O-surface labeled $Ru_{0.5}Mn_{0.5}O_2$ (b), and ^{18}O-surface labeled C-RuO_2 (c). DEMS signals of O_2 products for ^{18}O-surface labeled V_{Mn}-$Ru_{0.5}Mn_{0.5}O_{2-x}$ (d), ^{18}O-surface labeled $Ru_{0.5}Mn_{0.5}O_2$ (e), and ^{18}O-surface labeled C-RuO_2 (f) in the electrolyte using $H_2{}^{16}O$ as the solvent during three times of CV.

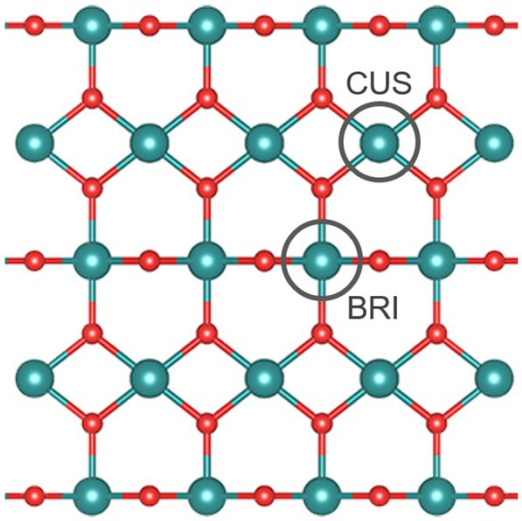

Figure S48. Two types of Ru site, CUS and BRI, on the terminated layer of RuO_2(110) surface.

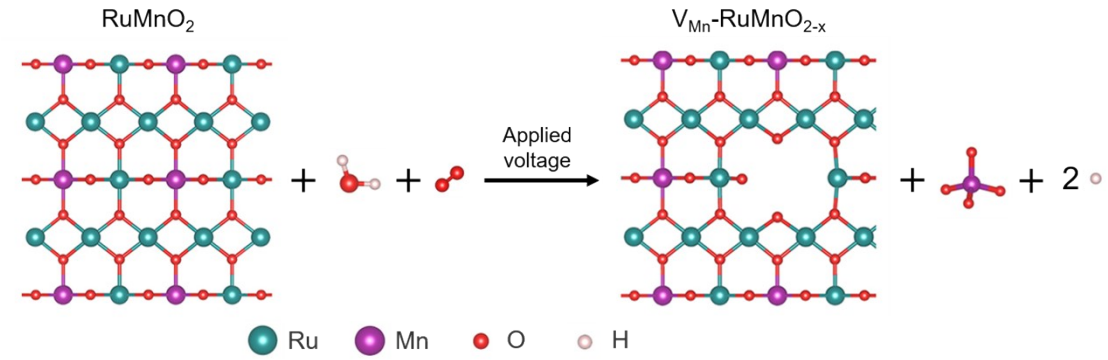

Figure S49. Atomistic structures showing the demetallation of Mn from $RuMnO_2(110)$ surface, using H_2O and O_2 as oxidants and MnO_4^- as the final dissolution product.

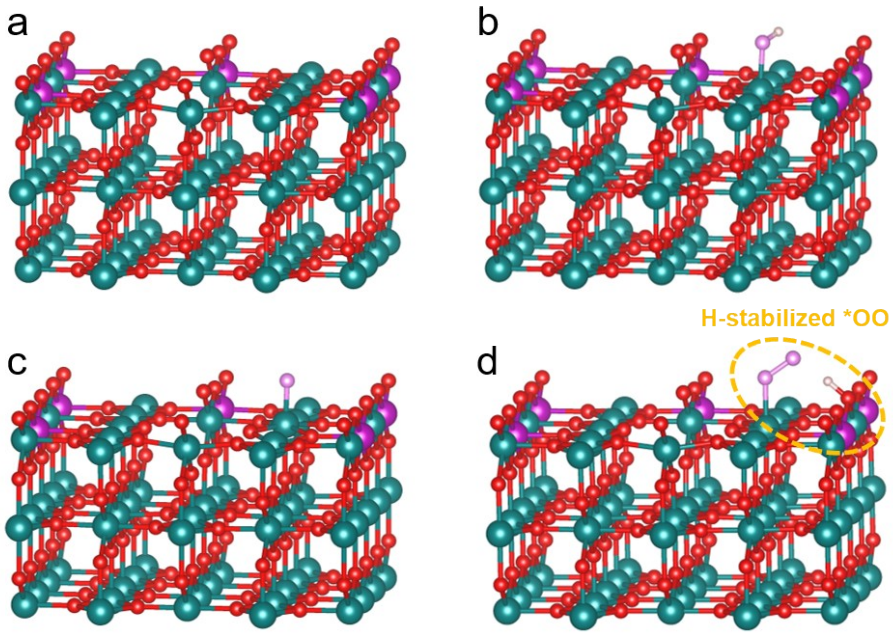

Figure S50. Ball and stick models of V_{Mn}-$RuMnO_{2-x}$(110) (a), OH adsorbed on V_{Mn}-$RuMnO_{2-x}$(110) (b), O adsorbed on the V_{Mn}-$RuMnO_{2-x}$(110) (c), and OOH adsorbed on the V_{Mn}-$RuMnO_{2-x}$(110) (d).

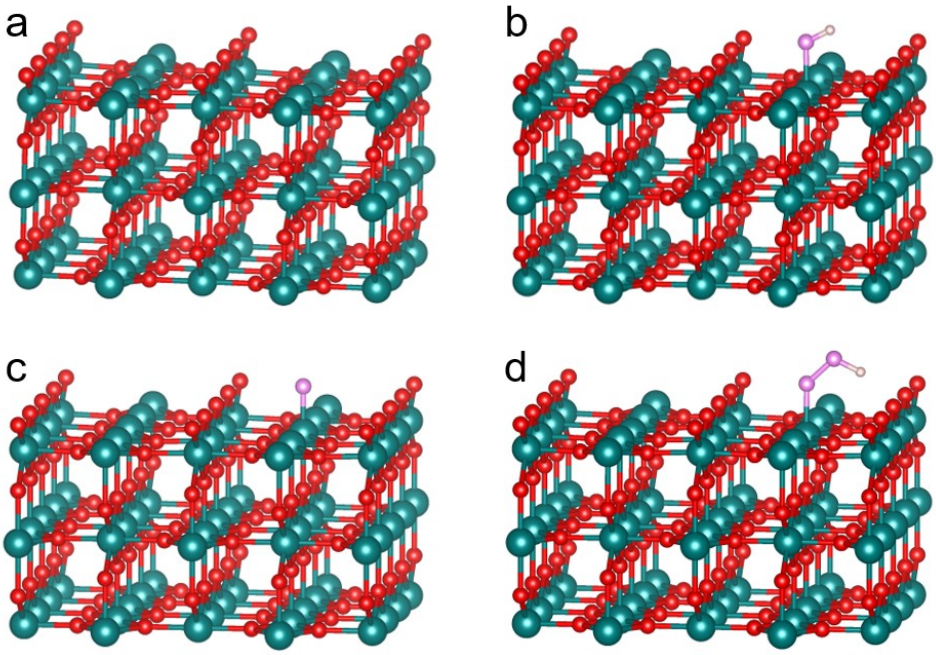

Figure S51. Ball and stick models of RuO_2(110) (a), OH adsorbed on RuO_2(110) (b), O adsorbed on the RuO_2(110) (c), and OOH adsorbed on the RuO_2(110) (d).

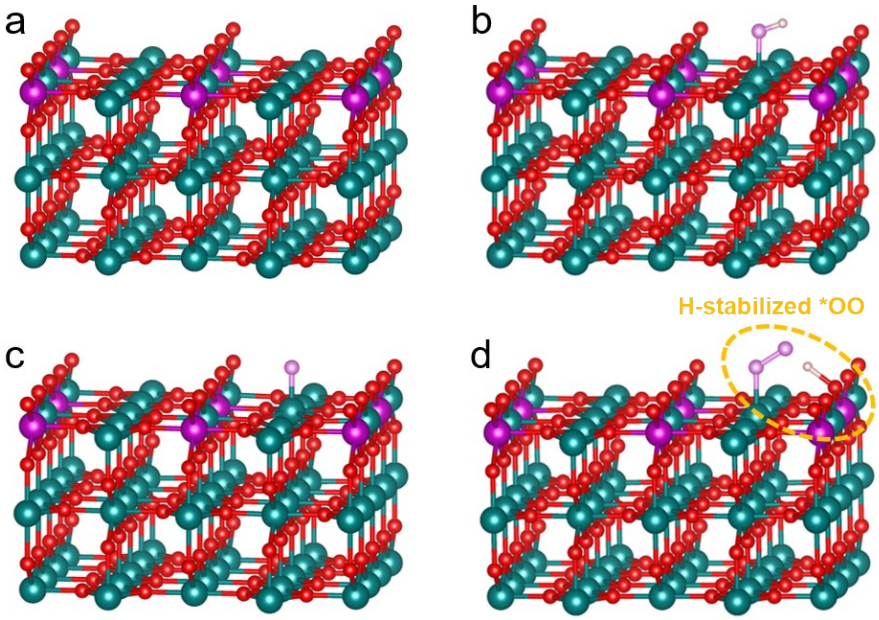

Figure S52. Ball and stick models of $RuMnO_2(110)$ (a), OH adsorbed on $RuMnO_2(110)$ (b), O adsorbed on the $RuMnO_2(110)$ (c), and OOH adsorbed on the $RuMnO_2(110)$ (d).

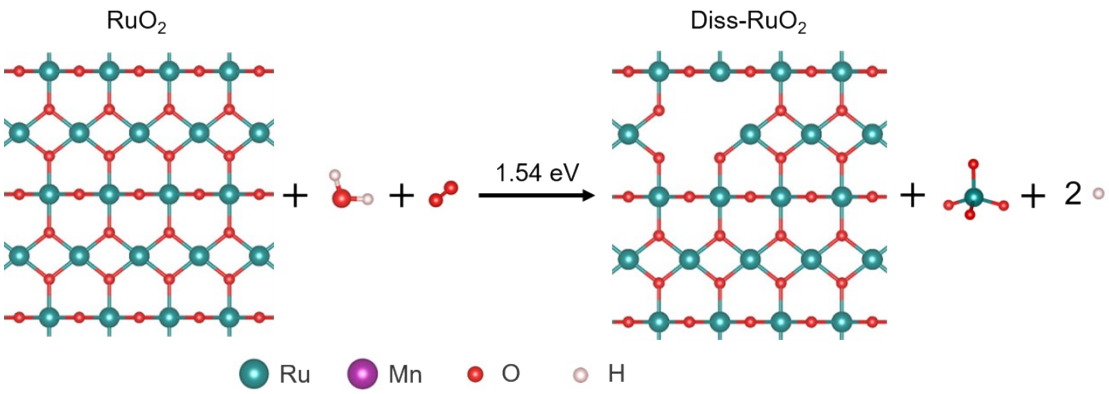

Figure S53. Atomistic structures showing the demetallation of Ru from RuO_2(110) surface, using H_2O and O_2 as oxidants and RuO_4 as the final dissolution product.

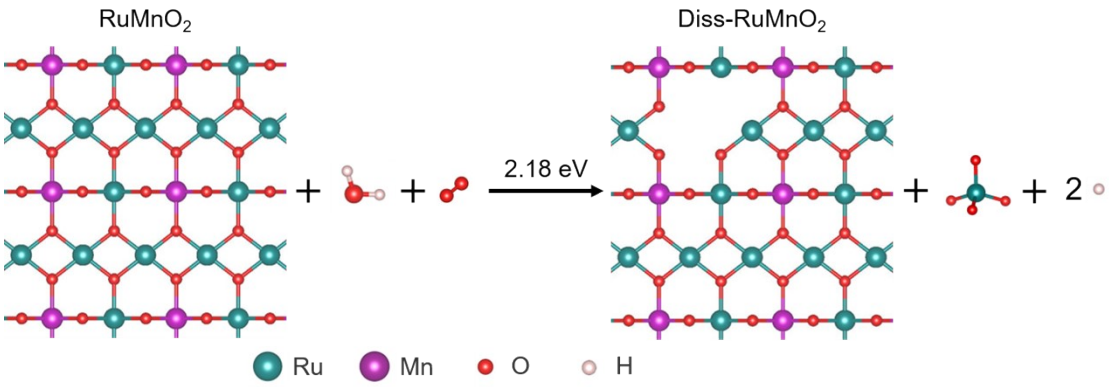

Figure S54. Atomistic structures showing the demetallation of Ru from $RuMnO_2$(110) surface, using H_2O and O_2 as oxidants and RuO_4 as the final dissolution product.

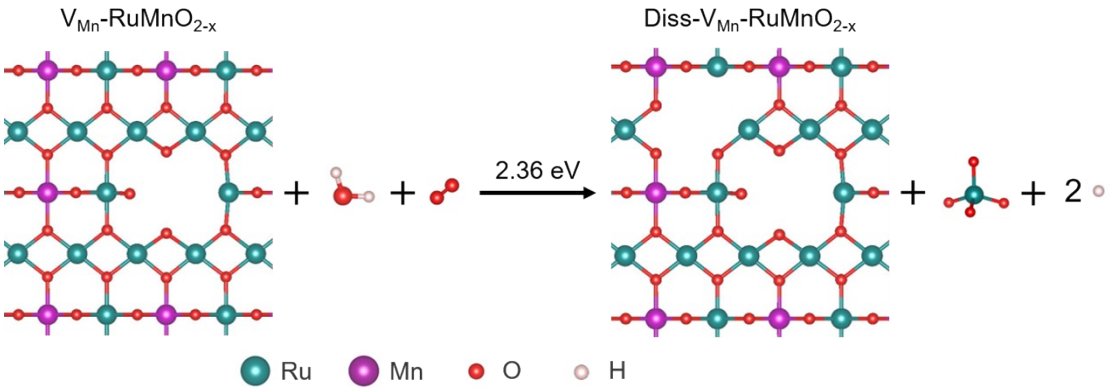

Figure S55. Atomistic structures showing the demetallation of Ru from V_{Mn}-$RuMnO_{2-x}$(110) surface, using H_2O and O_2 as oxidants and RuO_4 as the final dissolution product.

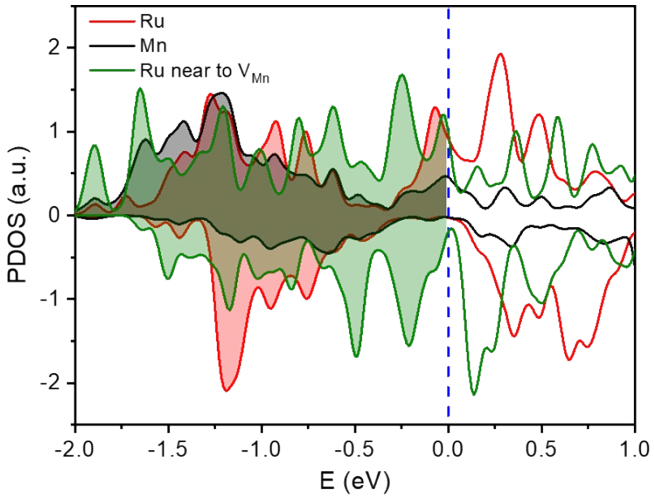

Figure S56. The projected densities of states (PDOS) of Mn and CUS Ru atom of $RuMnO_2$(110) and the CUS Ru atom nearby the Mn vacancy in V_{Mn}-$RuMnO_{2-x}$(110).

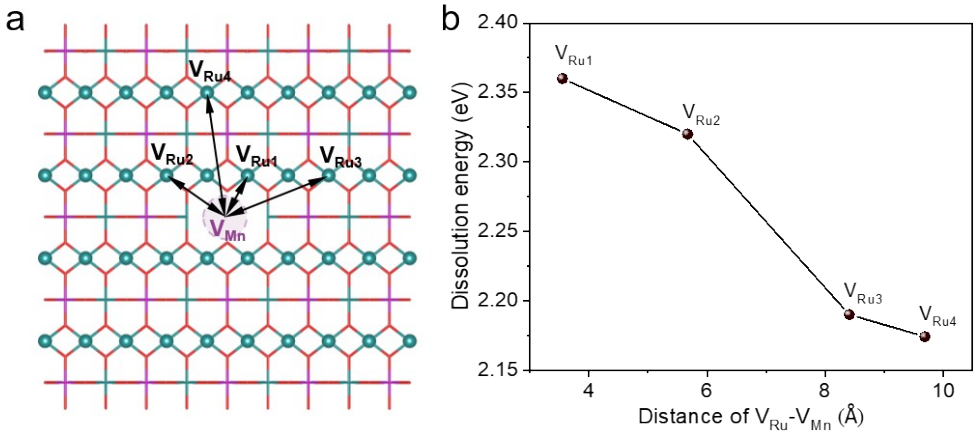

Figure S57. (a) Different distances between the V_{Mn} site to some nearby Ru atoms. (b) Calculated demetallation energies of four Ru atoms nearby the V_{Mn} site.

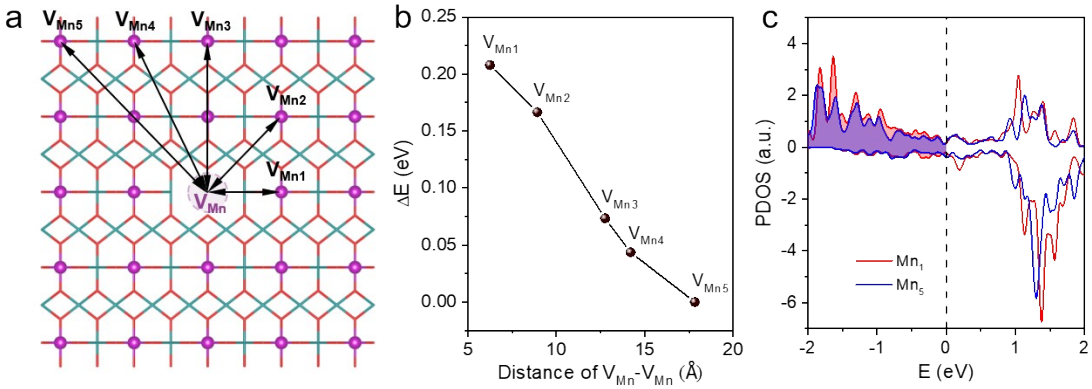

Figure S58. (a) Different distances between two Mn vacancies. (b) The calculated energies of surface models with different V_{Mn}-V_{Mn} distance. (c) The projected densities of states (PDOS) of Mn_1 (close to V_{Mn} site) and Mn_5 atoms (further away from V_{Mn} site).

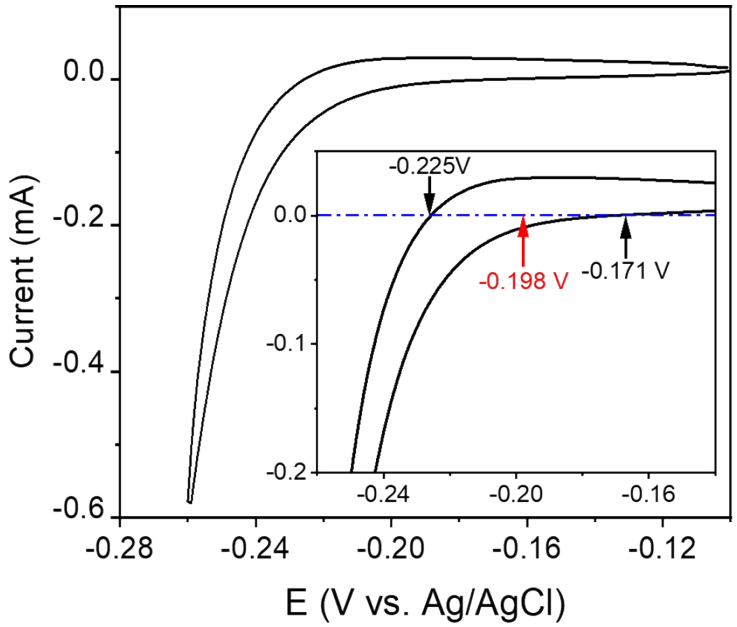

Figure S59. Calibration of the saturated Ag/AgCl electrode in 0.5 M H_2SO_4.

Table S1. Parameters obtained from the curve-fitting analysis of the EIS spectra. The double layer capacitance is used to account for the catalyst surface roughness and treated as the constant phase element (CPE), which is comprised of two components of CPE-P (the semicircle in the Nyquist plot) and CPE-T (pseudo capacitance).

	$Ru_{0.5}Mn_{0.5}O_2$	$Ru_1Mn_0O_2$	$Ru_0Mn_1O_2$	C-RuO_2
R_s (ohm)	6.371	9.623	4.423	7.225
R_{ct} (ohm)	13.37	26.92	76847	554.4
CPE-T	0.020071	0.032909	3.2955E-5	0.0020776
CPE-P	0.88371	0.89388	0.83478	0.9675

Table S2. The Ru/Mn atomic ratios in $Ru_yMn_{1-y}O_2$ (y=0.1, 0.3, 0.5, 0.7, 0.9) according to ICP-AES analysis.

Samples	$Ru_{atom}/(Ru_{atom}+Mn_{atom})$ (%)
$\mathbf{Ru_{0.1}Mn_{0.9}O_2}$	6.4
$\mathbf{Ru_{0.3}Mn_{0.7}O_2}$	35.9
$\mathbf{Ru_{0.5}Mn_{0.5}O_2}$	54.3
$\mathbf{Ru_{0.7}Mn_{0.3}O_2}$	69.9
$\mathbf{Ru_{0.9}Mn_{0.1}O_2}$	89.2

Table S3. Comparison of activities and stability of recently reported OER electrocatalysts in acidic media.

No	Catalyst	Substrate	Electrolyte	Overpotential (mV@10 mA m^{-2})	Stability (h@10 mA m^{-2})	Ref.
	$Ru_{0.5}Mn_{0.5}O_2$	GCE	0.5 M H_2SO_4	166	2500	This work
1	**$Li_{0.52}RuO_2$**	GCE	0.5 M H_2SO_4	156	70	*(40)*
2	**BCN-0.5Ru**	GCE	0.5 M H_2SO_4	164	12	*(41)*
3	**12Ru/MnO_2**	GCE	0.1 M $HClO_4$	161	200	*(42)*
4	**$W_{0.2}Er_{0.1}Ru_{0.7}O_{2-\delta}$**	Carbon paper	0.5 M H_2SO_4	168	500	*(43)*
5	**py-RuO_2:Zn**	Ti plate	0.5 M H_2SO_4	173	1,000	*(44)*
6	**$Cr_{0.2}Ru0_{.8}O_{2-x}$**	GCE	0.1 M $HClO_4$	170	2000	*(45)*
7	**Ru@V-RuO_2/C HMS**	GCE	0.5 M H_2SO_4	176	25	*(46)*
8	**$Ru_{0.85}Zn_{0.15}O_{2-\delta}$**	GCE	0.5 M H_2SO_4	190	50	*(47)*
9	**$Re_{0.06}Ru_{0.94}O_2$**	GCE	0.1 M $HClO_4$	190	200	*(48)*
10	**RuFe@CF**	Carbon felt	0.5 M H_2SO_4	188	620	*(36)*
11	**Ru/RuS_2**	GCE	0.5 M H_2SO_4	201	24	*(49)*
12	**Ru-UiO-67-bpydc**	GCE	0.5 M H_2SO_4	200	115	*(50)*
13	**C-RuO_2-RuSe-5**	GCE	0.5 M H_2SO_4	212	30	*(51)*
14	**Ni-RuO_2**	GCE	0.1 M $HClO_4$	214	200	*(2)*
15	**Ru_1-Pt_3Cu**	GCE	0.1 M $HClO_4$	220	28	*(52)*
16	**Ru/Co–N–C**	Carbon fiber paper	0.5 M H_2SO_4	232	20	*(53)*
17	**$Ru_5W_1O_x$**	GCE	0.5 M H_2SO_4	235	550	*(54)*
18	**Y_2MnRuO_7**	GCE	0.1 M $HClO_4$	260	45	*(39)*

Table S4. The element content of $Ru_{0.5}Mn_{0.5}O_2$ catalyst before test, after 1 h test, after 10 h test, and after 50 h test according to EDS analysis.

Samples	Ru ($_{atom}$%)	Mn ($_{atom}$%)	O ($_{atom}$%)	Total	$Ru_{atom}/(Ru_{atom}+Mn_{atom})$ (%)
$Ru_{0.5}Mn_{0.5}O_2$ Before test	15.71	10.67	73.62	100.00	59.55
$Ru_{0.5}Mn_{0.5}O_2$ After 1 h test	14.67	9.66	75.67	100.00	60.30
$Ru_{0.5}Mn_{0.5}O_2$ After 10 h test	14.25	6.89	78.86	100.00	67.41
$Ru_{0.5}Mn_{0.5}O_2$ After 50 h test	12.91	5.33	81.76	100.00	70.78

Table S5. The atomic concentration of Ru, Mn, and O in $Ru_{0.5}Mn_{0.5}O_2$ catalyst before test, after 1 h test, after 10 h test, and after 50 h test according to XPS analysis.

Samples	Ru ($_{atomic\ conc.}$%)	Mn ($_{atomic\ conc.}$%)	O ($_{atomic\ conc.}$%)	$Ru_{atom}/(Ru_{atom}+Mn_{atom})$ (%)
$Ru_{0.5}Mn_{0.5}O_2$ Before test	4.2	4.5	21.2	48.28
$Ru_{0.5}Mn_{0.5}O_2$ After 1 h test	2.1	2.1	11	50.00
$Ru_{0.5}Mn_{0.5}O_2$ After 10 h test	2.9	1.5	14.5	65.91
$Ru_{0.5}Mn_{0.5}O_2$ After 50 h test	1.2	0.6	8.8	66.67

Table S6. Structural parameters of $Ru_{0.5}Mn_{0.5}O_2$ catalyst before test, after 10 h test, after 20 h test, and after 50 h test, which extracted from fitting results for Ru K-edge EXAFS.

Samples	Bond	Coordination number (CN)	Bond length R (Å)	σ^2 (Å) x 10^{-3}	R factor
$Ru_{0.5}Mn_{0.5}O_2$ Before test	Ru-O	4.95	1.939	1.17	0.0001062
	Ru-M	5.74	3.403	1.29	0.0008714
$Ru_{0.5}Mn_{0.5}O_2$ After 10 h test	Ru-O	4.87	1.940	1.95	0.0001493
	Ru-M	5.55	3.410	1.09	0.0008991
$Ru_{0.5}Mn_{0.5}O_2$ After 20 h test	Ru-O	4.89	1.938	1.01	0.0001693
	Ru-M	5.42	3.421	1.65	0.0000867
$Ru_{0.5}Mn_{0.5}O_2$ After 50 h test	Ru-O	4.88	1.934	1.99	0.0001997
	Ru-M	5.28	3.399	1.46	0.0007210

σ^2: Debye-Waller factor; R factor: goodness of fit.

Table S7. Structural parameters of $Ru_{0.5}Mn_{0.5}O_2$ catalyst before test, after 10 h test, after 20 h test and after 50 h test, which extracted from fitting results for Mn K-edge EXAFS.

Samples	Bond	Coordination number (CN)	Bond length R (Å)	σ^2 (Å) x 10^{-3}	R factor
$Ru_{0.5}Mn_{0.5}O_2$ Before test	Mn-O	5.27	1.912	3.06	0.0025377
	Mn-M	5.53	2.934	2.76	0.002817
$Ru_{0.5}Mn_{0.5}O_2$ After 10 h test	Mn-O	5.37	1.910	3.18	0.0026288
	Mn-M	5.23	2.924	2.53	0.003080
$Ru_{0.5}Mn_{0.5}O_2$ After 20 h test	Mn-O	5.24	1.908	3.12	0.0026008
	Mn-M	4.98	2.909	2.28	0.002291
$Ru_{0.5}Mn_{0.5}O_2$ After 50 h test	Mn-O	5.34	1.911	3.41	0.0021332
	Mn-M	5.04	2.934	2.32	0.003575

σ^2: Debye-Waller factor; R factor: goodness of fit.

Table S8. Structural parameters of V_{Mn}-$Ru_{0.5}Mn_{0.5}O_{2-x}$ under different potentials extracted from fitting results for Ru K-edge EXAFS.

Samples	Bond	Coordination number (CN)	Bond length R (Å)	σ^2 (Å) x 10^{-3}	R factor
OCV	Ru-O	4.38	1.948	1.32	0.0003462
1.2 V	Ru-O	4.57	1.945	1.36	0.0005307
1.4 V	Ru-O	4.40	1.949	1.14	0.0004087
1.5 V	Ru-O	4.51	1.946	1.38	0.0006614
1.55 V	Ru-O	4.54	1.951	1.88	0.0010144
1.6 V	Ru-O	4.34	1.949	1.30	0.0004048
1.55 V-back	Ru-O	4.48	1.948	1.34	0.0004428
1.5 V-back	Ru-O	4.45	1.949	1.17	0.0004556
1.4 V-back	Ru-O	4.54	1.950	1.04	0.0004543
1.2 V-back	Ru-O	4.49	1.950	1.13	0.0004220
OCV-back	Ru-O	4.56	1.948	1.03	0.0004882

σ^2: Debye-Waller factor; R factor: goodness of fit.

Table S9. Structural parameters of V_{Mn}-$Ru_{0.5}Mn_{0.5}O_{2-x}$ under different potentials extracted from fitting results for Mn K-edge EXAFS.

Samples	Bond	Coordination number (CN)	Bond length R (Å)	σ^2 (Å) x 10^{-3}	R factor
OCV	Mn-O	5.39	1.934	6.87	0.0006578
1.2 V	Mn-O	5.33	1.936	6.70	0.0010921
1.4 V	Mn-O	5.45	1.935	6.94	0.0008605
1.5 V	Mn-O	4.92	1.933	7.06	0.0007230
1.55 V	Mn-O	5.25	1.936	6.76	0.0012595
1.6 V	Mn-O	5.04	1.938	6.86	0.0003658
1.55 V-back	Mn-O	5.41	1.934	6.80	0.0013920
1.5 V-back	Mn-O	5.53	1.936	6.70	0.0008103
1.4 V-back	Mn-O	5.58	1.938	7.18	0.0013130
1.2 V-back	Mn-O	5.37	1.938	6.80	0.0005258
OCV-back	Mn-O	5.25	1.934	6.59	0.0004510

σ^2: Debye-Waller factor; R factor: goodness of fit.

Table S10. The Gibbs free energy (eV) changes on RuO_2(110), $RuMnO_2$(110), and V_{Mn}-$RuMnO_{2-x}$(110) during the OER process.

Catalyst	ΔG_1	ΔG_2	ΔG_3	ΔG_4
RuO_2(110)	0.63	0.95	**2.04**	1.30
$RuMnO_2$(110)	0.75	0.8	**1.91**	1.46
V_{Mn}-$RuMnO_{2-x}$(110)	0.50	1.00	1.69	**1.73**

References

1 X. Cui, P. Ren, C. Ma, J. Zhao, R. Chen, S. Chen, N. P. Rajan, H. Li, L. Yu, Z. Tian and D. Deng, *Adv. Mater.*, 2020, **32**, 1908126.

2 J. Chen, Y. Ma, T. Huang, T. Jiang, S. Park, J. Xu, X. Wang, Q. Peng, S. Liu, G. Wang and W. Chen, *Adv. Mater.*, 2024, **36**, 2312369.

3 H. Liu, Z. Zhang, J. Fang, M. Li, M. G. Sendeku, X. Wang, H. Wu, Y. Li, J. Ge, Z. Zhuang, D. Zhou, Y. Kuang and X. Sun, *Joule*, 2023, **7**, 558-573.

4 J. Kwon, S. Sun, S. Choi, K. Lee, S. Jo, K. Park, Y. K. Kim, H. B. Park, H. Y. Park, J. H. Jang, H. Han, U. Paik and T. Song, *Adv. Mater.*, 2023, **35**, 2300091.

5 C. Liu, Y. Jiang, T. Wang, Q. Li and Y. Liu, *Adv. Sci.*, 2023, **10**, 2207429.

6 D. Zhang, M. Li, X. Yong, H. Song, G. I. N. Waterhouse, Y. Yi, B. Xue, D. Zhang, B. Liu and S. Lu, *Nat. Commun.*, 2023, **14**, 2517.

7 Y. Wang, X. Lei, B. Zhang, B. Bai, P. Das, T. Azam, J. Xiao and Z. S. Wu, *Angew. Chem. Int. Ed.*, 2023, **63**, e202316903.

8 L. Deng, S. F. Hung, Z. Y. Lin, Y. Zhang, C. Zhang, Y. Hao, S. Liu, C. H. Kuo, H. Y. Chen, J. Peng, J. Wang and S. Peng, *Adv. Mater.*, 2023, **35,** 2305939.

9 Z. L. Zhao, Q. Wang, X. Huang, Q. Feng, S. Gu, Z. Zhang, H. Xu, L. Zeng, M. Gu and H. Li, *Energy Environ. Sci.*, 2020, **13**, 5143-5151.

10 A. M. Harzandi, S. Shadman, A. S. Nissimagoudar, D. Y. Kim, H. D. Lim, J. H. Lee, M. G. Kim, H. Y. Jeong, Y. Kim and K. S. Kim, *Adv. Energy Mater.*, 2021, **11**, 2003448.

11 Y. Xue, J. Zhao, L. Huang, Y.-R. Lu, A. Malek, G. Gao, Z. Zhuang, D. Wang, C. T. Yavuz and X. Lu, *Nat. Commun.*, 2023, **14,** 8093.

12 X. Long, B. Zhao, Q. Zhao, X. Wu, M.-N. Zhu, R. Feng, M. Shakouri, Y. Zhang, X. Xiao, J. Zhang, X.-Z. Fu and J.-L. Luo, *Appl. Catal. B Environ.*, 2024, **343,** 123559.

13 D. Wu, K. Kusada, S. Yoshioka, T. Yamamoto, T. Toriyama, S. Matsumura, Y. Chen, O. Seo, J. Kim, C. Song, S. Hiroi, O. Sakata, T. Ina, S. Kawaguchi, Y. Kubota, H. Kobayashi and H. Kitagawa, *Nat. Commun.*, 2021, **12,** 1145.